# Ionic Conducting Lanthanide Oxides

Gin-ya Adachi, Nobuhito Imanaka,* and Shinji Tamura

*Department of Applied Chemistry, Faculty of Engineering, Osaka University, Osaka 565-0871, Japan*

*Received November 28, 2001*

## Contents



## I. Introduction

"Solid electrolytes" are functional materials that conduct electric charge accompanied by mass and are therefore ionic conductors. This feature is definitely different from electronic conduction in materials such as metals and semiconductors, where charge alone is transported. Solid electrolytes belong to the field of ionics in the solid state, and "solid state ionics" is regarded as an interdisciplinary science.

As early as the end of the 19th century, the relationship between the current passing through solids and the resulting chemical changes were found to obey Faraday's law.[1] One of the well-known solid electrolytes, stabilized zirconia using one of the rare earths as an additive, was first developed in 1897 as a light source by a resistive heating and was called a "Nernst glower". A more complete understanding of electrical conduction in such ionic solids was successfully realized in the thesis of Wagner in 1943.[2] During the period between 1897 and 1943, several important discoveries concerning ionic conducting behavior in solids were reported, mainly in halide compounds. In particular, very high ion conducting characteristics were obtained for silver iodide (AgI) found by Tubandt.[3] Silver iodide undergoes a structural phase transformation at 149 °C from the low-temperature $\gamma$ phase to the high temperature $\alpha$ phase. Coincident with this transition, the $Ag^+$ ion conductivity jumps more than 5 orders of magnitude to reach a value almost equivalent to the liquid AgI phase. In the course of trying to stabilize the high $Ag^+$ ion conductive $\alpha$-AgI phase down to room temperature, compounds with $Ag^+$ and $I^-$ ions such as $RbAg_4I_5$ were synthesized in 1965.[4] However, $RbAg_4I_5$ is very unstable and has not yet found commercial application. At about the same time a lanthanum compound, $LaF_3$ which shows $F^-$ ion conducting characteristics, was reported.[5] Another very important discovery after 1943 was the two-dimensional high $Na^+$ ion conducting $\beta$-alumina found by Kummer et al.,[6] despite knowledge of the existence of $\beta$-alumina dating back to the 1930s. Since the mobile ion species has mass and occupies volume, it was recognized that these characteristics had to be taken into account to improve transport through a three-dimensional tunnel structure. One of the optimum candidate structures, which is generally accepted to be suitable for ion migration, was artificially designed by Goodenough et al. in 1976 in order to realize a high ion conduction.[7] This "tailored solid electrolyte", with chemical formula $Na_{1+x}Zr_2P_{3-x}Si_xO_{12}$, has been named NASICON ($Na^+$ super ionic conductor).

In the 1980s, solid electrolytes with $H^+$ as the mobile ion, and therefore called proton conductors, attracted a lot of interest. Iwahara et al.[8] developed a solid electrolyte compound for operation at high temperature based on the perovskite structure in which a lanthanoid element plays an important role in the conduction process. After that, various types of perovskite-based ion conductors were eagerly investigated not only for proton but also for oxide anion conductors.

With regard to the practical applications, yttria-stabilized zirconia was applied as an oxygen sensor around 1976, and a fluorine ion sensor with a $LaF_3$−$EuF_2$ single-crystal solid solution has been already

* To whom correspondence should be addressed. Phone: +81-6-6879-7353. Fax: +81-6-6879-7354. E-mail: imanaka@chem.eng.osaka-u.ac.jp.

10.1021/cr0103064 CCC: $39.75 
Published on Web 05/15/2002

Gin-ya Adachi was born in Osaka, Japan, in 1938. He received his Bachelor's degree in Chemistry at Kobe University. He then obtained his M.E. (1964) and Ph.D. (1967) degrees in Applied Chemistry from Osaka University. He joined the faculty at Osaka University in 1967, and now he is Professor Emeritus. His main research interests are inorganic materials containing rare-earth elements. He has been the President of The Rare Earth Society of Japan since 1995.

Nobuhito Imanaka was born in Kawanishi, Hyogo, in 1958. He earned his B.E. (1981) and M.E. (1983) degrees in Applied Chemistry from Osaka University. He then obtained his Ph.D. degree from Osaka University in 1986. He has been a member of the faculty at Osaka University since 1988, and he is Associate Professor. His main research fields include rare earths and functional materials such as solid electrolytes and chemical sensors.

Shinji Tamura was born in Osaka, Japan, in 1972. He received his B.E. (1997) degree in Applied Chemistry from Osaka University. He then obtained his M.E. (1999) and Ph.D. (2001) degrees in Materials Chemistry, Osaka University, and now he is a postdoctoral fellow at Osaka University.

commercialized. A proton conductor application is a hydrogen sensor at high temperatures, such as that required for molten metals, and has been already put on the market. Furthermore, $Li^+$ ion conductors and oxide ion conductors are greatly expected to be utilized for the all solid-state rechargeable batteries and solid oxide fuel cells (SOFCs).

The rare earths' (including lanthanoids) contribution is divided in three categories: first as the main constituent of the solid electrolytes; second is to function as additives to improve the ion conducting characteristics; third is rare earths (including lanthanoids) cation migrating solid electrolytes, and these electrolytes are exactly rare-earth solid electrolytes playing the main role in solid state ionics field.[9,10]

In this review article the sections are divided according to the three categories and each subsection is divided according to the individual migrating ion species. In some cases, ion−electron mixed conductors are covered in the solid state ionics field. However, in this review we mainly focus on only pure ion conducting solid electrolytes. In addition, strictly speaking, lanthanides include only 14 elements from Ce to Lu. Here, we use the abbreviation Ln (lanthanoids) and R for La + lanthanides and rare earths of Sc, Y, La, and lanthanides.

## *II. Solid Electrolytes with Rare Earths as Framework Elements*

### A. Cationic Conductors

#### *1. Lithium Ion Conductors*

**a. $Li_{3x}La_{2/3-x}\square_{1/3-2x}TiO_3$ (□: vacancies).** A perovskite-type material, whose general formula is described as $ABO_3$ (A, larger cation (12-coordinate); B, smaller cation (6-coordinate)) and containing two different sized cations, can stably hold the structure even with a large amount of oxygen-deficient structure. It is well-known that a huge number of materials with the perovskite structure exist on and in the earth. One of most remarkable properties of the perovskite compounds in the solid state ionics field is that various compositions can be realized by the substitution of A or B sites for aliovalent cations, and the lattice size can be widely adjusted by the replacement. Consequently, a large number of solid electrolytes with the perovskite-type structure has been synthesized and studied. In 1984, $Li_xLn_{1/3}Nb_{1-x}Ti_xO_3$ (Ln = La, Nd) was reported to be a lithium ion conductor with the perovskite structure by Latie et al.[11] Since then, several studies have reported $Li^+$ ion conductivity in perovskite-type solid electrolytes. In recent years, an extraordinarily high $Li^+$ ionic conductivity even at room temperature was observed for $Li_{3x}La_{2/3-x}\square_{1/3-2x}TiO_3$ (where □ denotes a vacancy), which belongs to the series $Li_{0.5}Ln_{0.5}TiO_3$ (Ln = La, Pr, Nd, and Sm).[12,13] The $Li^+$ ion conductivity for $Li_{0.5}Ln_{0.5}TiO_3$ (Ln = La, Pr, Nd, Sm) is presented in Figure 1. The conductivity at room temperature for the La system is ca. $10^{-3}$ S·cm$^{-1}$, and the value is 3 orders of magnitude higher than that for the Pr system. Figure 2 depicts the perovskite parameter ($a_p$) dependencies of the conductivity and the activation energy of conduction, which is calculated from the Arrhenius plots in the relationship log($\sigma$T) versus

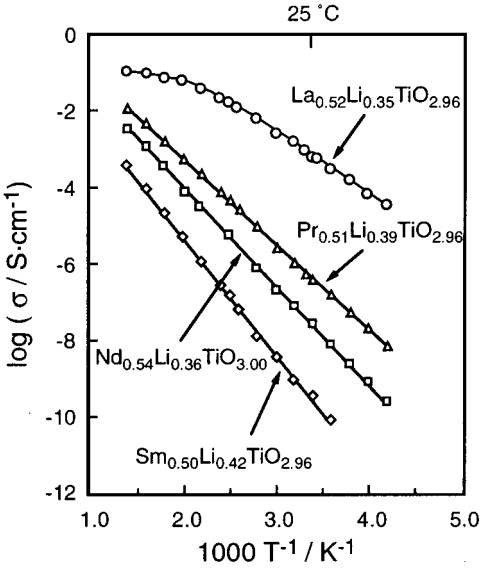


**Figure 1.** $Li^+$ ion conductivity for $Li_{0.5}Ln_{0.5}TiO_3$ (Ln = La, Pr, Nd, Sm). (Reprinted with permission from ref 12. Copyright 1997 Elsevier Science Ltd.)

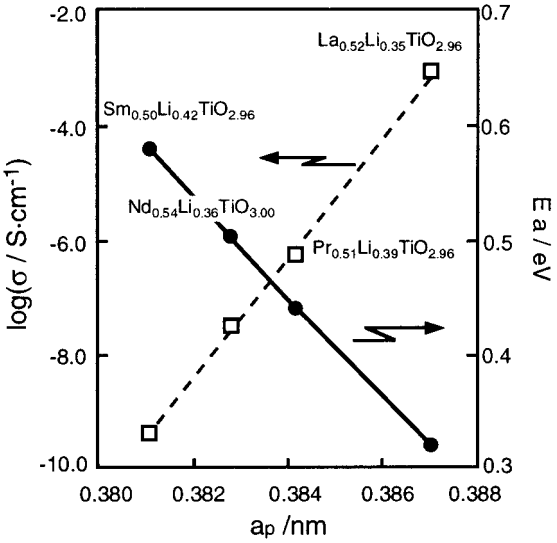


**Figure 2.** Perovskite parameter $a_p$ dependencies of the conductivity and the activation energy, which is calculated from the Arrhenius plot relationship between $\log(\sigma T) - 1/T$. (Reprinted with permission from ref 12. Copyright 1997 Elsevier Science Ltd.)

$1/T$. Here, $a_p$ represents a cube root of the primitive perovskite cell; for example, the orthorhombic perovskite structure has a relation such as $a_0 \approx b_0 \approx \sqrt{2}a_p$, $c_0 \approx 2a_p$. Figure 2 shows that $Li^+$ ion conductivity increases and the activation energy decreases with increasing $a_p$ for $Li_{0.5}Ln_{0.5}TiO_3$. Among the $Li_{3x}Ln_{2/3-x}\square_{1/3-2x}TiO_3$ group, the La series shows the highest conductivity because the largest lanthanum ion provides the largest lattice size and, as a result, the widest conducting pathway in the perovskite structure.

Ion conduction is known to occur through the conduction path composed of $Li^+$ ions and the vacancies. The $Li^+$ ions in $Li_{3x}La_{2/3-x}\square_{1/3-2x}TiO_3$ migrate through the bottleneck which is defined as the 3c site (the space group is $Pm3m$) surrounded by four oxide ions in the structure as shown in Figure 3. A high $Li^+$ ion conductivity is of great interest because the

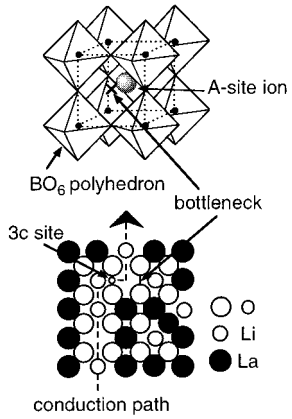


**Figure 3.** $Li^+$ ion migration model in $Li_{3x}La_{2/3-x}\square_{1/3-x}TiO_3$ through the bottleneck which is defined as the 3c site surrounded by four oxide ions. (Reprinted with permission from ref 14. Copyright 1999 The Ceramic Society of Japan.)

conducting paths of the ions may exist in the vicinity of the A-site of the perovskite structure since the Coulomb potential for the B-site ions may be quite deep and does not allow the migration of cations through the B-site. The A-site defect concentration and the lattice volume of $Li_{3x}La_{2/3-x}\square_{1/3-2x}TiO_3$ series can change with $x$, which means that the $Li^+$ ion conductivity can also vary with $x$.

By using molecular dynamics (MD) simulation, the optimum lattice size for $Li^+$ ion conduction was estimated. The suitable lattice size predicted is larger than the actual lattice size in $La_{0.6}Li_{0.2}TiO_3$, and this indicates that the $Li^+$ ion conductivity in $La_{0.6}Li_{0.2}TiO_3$ is expected to become several times higher by expanding the framework of the structure.[14]

The study of lithium ion conductivity in perovskite-type oxides is still important in solid-state chemistry and solid-state ionics as suggested by the following experimental results: (1) Cation conductivity other than for a proton is not yet known in the perovskite-type oxides. (2) Higher lithium ion conductivity, which is comparable to that of $Li^+$–$\beta$-alumina, is achieved in a system with higher crystal symmetry. (3) The importance of the vacancy/charge carrier ratio has been experimentally confirmed. (4) A site percolation model (see the ref 15) has been found to explain the characteristics of the lithium ion conducting path through A sites. (5) Activation energy is simply related to the size of lattice, i.e., the bottleneck formed by the four oxygen ions. (6) Covalency of the host lattice is indispensable for the migration of lithium ions. However, these solid electrolytes are easily reduced due to the inclusion of Ti atoms, and therefore, improvement of the chemical stability of these materials is required for any application.

Interest in the $Li^+$ ion conducting behavior of the $Li_{3x}Ln_{2/3-x}\square_{1/3-2x}TiO_3$ series led to extensive examination of the $Li_{3x}La_{2/3-x}\square_{1/3-2x}TiO_3$ series.[16–19] Figure 4 shows the Li concentration dependencies of the conductivity for $Li_{3x}La_{2/3-x}\square_{1/3-2x}TiO_3$ at various temperatures. The highest conductivity was obtained for $3x = 0.34$ ($Li_{0.34}La_{0.55}\square_{0.11}TiO_3$) at all temperatures measured. The reason for obtaining the highest $Li^+$ conductivity in this perovskite structure was explained by site percolation theory.

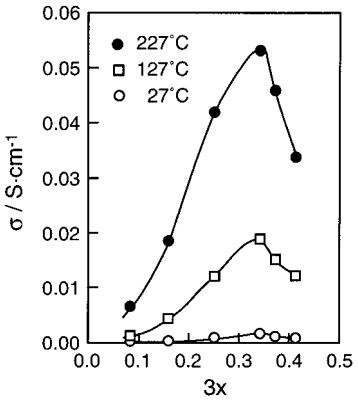


**Figure 4.** $Li^+$ ion concentration dependencies of the $Li^+$ conductivity for $Li_{3x}La_{2/3-x}\square_{1/3-x}TiO_3$. (Reprinted with permission from ref 19. Copyright 1996 Elsevier Science B.V.)

However, these $Li^+$ ion conductors with perovskite structure were mainly discussed from the bulk conductivity viewpoint despite the samples being in a polycrystalline state. Therefore, for a complete understanding of the total ion conduction behavior, detailed investigations of the ion conductivity at grain boundaries are required in addition to the bulk conductivity.

**b. $Li_xLn_{1/3}Nb_{1-x}Ti_xO_3$ (Ln = La, Nd).** The compound with the general formula $Ln_{1/3}NbO_3$ (Ln = La, Ce, Pr, Nd) was isolated by Dyer and White in 1964,[20] and the crystal structure of this series of niobates was determined by Iyer and Smith.[21] The structure of these compounds related to the perovskite-type structure and Nb is octahedrally coordinated with oxygen, and each octahedron shares corners in three directions. Parallel to the *ab* plane, one site is completely empty (○) and one is statistically occupied with a 2/3 filling factor by Ln (●) as shown in Figure 5. A higher conductivity is obtained for the above-

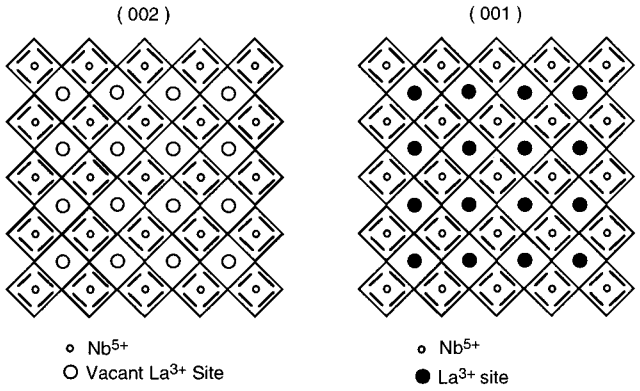


**Figure 5.** Crystal structure of $La_{1/3}NbO_3$ parallel to the *ab* plane. One site is completely empty (○) and one is statistically occupied by 2/3 of Ln (●). (Reprinted with permission from ref 113. Copyright 1988 Pergamon Press.)

mentioned lithium compounds in comparison with the case for $Na_xLn_{1/3}Nb_{1-x}Ti_xO_3$ (Ln = La, Nd). The highest $Li^+$ ion conductivity was obtained for $Li_xLa_{1/3}Nb_{1-x}Ti_xO_3$ ($x = 0.1$). However, the value (ca. $10^{-5}$ S·cm$^{-1}$ at room temperature) was 2 orders of magnitude lower than that for the above-mentioned $Li_{0.5}La_{0.5}TiO_3$. These above-mentioned results clearly indicate that the steric parameters greatly affect the conductivity characteristics. From the structural and NMR considerations, essentially two-dimensional $Li^+$ ion motion in the almost empty ○ planes is predominant. However, some motions through ● vacancies are also expected in addition to the motion between ○ and ●.[11]

**c. $LiLnSiO_4$.** The lithium rare-earth silicates, with a general composition described as $LiLnSiO_4$ (Ln = La, Nd, Sm, Eu, Gd, Dy), were reported as another type of $Li^+$ conducting solid electrolyte with high $Li^+$ ion conductivity of $(2-4) \times 10^{-3}$ S·cm$^{-1}$ at 600 °C.[22-24] The crystal structure of $LiLnSiO_4$ was refined to be an apatite-type structure by Sato et al.[22,23] The compounds with Ln = La−Dy are hexagonal, while those with Ln = Ho−Lu and Y are orthorhombic. These materials include the silicon-rich component in the grain boundaries. For applying the apatite chemical formula to the samples, the bulk composition can be expressed as $Li_xLn_{10-x}Si_6O_{24}O_{3-x}$ ($1 \leq x \leq 3$). From Rietveld analysis of $Li_xLn_{10-x}Si_6O_{24}O_{3-x}$, the compounds can be divided into two groups: one is the La, Nd series and Sm set of compounds which has a high occupation factor of Li and a low vacancy concentration with hexagonal symmetry. The other is Eu, Gd, and Dy systems having the opposite features with respect to occupation factor and vacancy concentration. The bulk conductivity was investigated, and the author reported that both high lithium occupation and vacancy are necessary for achieving relatively high $Li^+$ conductivity. However, the total conductivity including grain boundary conductivity reported in another paper[24] shows a different order of magnitude than the bulk conductivity. Therefore, the influence of grain boundary seems to be large for these compounds and should be investigated further.

**d. $YPO_4$−$Li_3PO_4$.** The $Y_{0.8}Li_{0.6}PO_4$−$Li_3PO_4$ mixed phase has a conductivity of $3.7 \times 10^{-2}$ S·cm$^{-1}$ at 600 °C, and from electrolysis and concentration cell methods, the $Y_{0.8}Li_{0.6}PO_4$−$Li_3PO_4$ phase was confirmed to be predominantly a $Li^+$ ion conducting solid electrolyte.[25] A $Na_3PO_4$-doped $YPO_4$ phase was also prepared, but they do not make a solid solution. This is ascribed to the large difference in ionic radius between Y (0.1040 nm; coordination number (CN) = 6[26]) and Na (0.1160 nm; CN = 6[26]).

### *2. Proton Conductors*

**a. Perovskite-Structured Strontium or Barium Cerates ($SrCeO_3$, $BaCeO_3$).** Pure strontium cerate, $SrCeO_3$, does not show any proton conduction at all. The electrical conductivity of the cerate is very low, indicating that the cerate is almost an insulating material. However, by replacing the tetravalent Ce for trivalent rare earths, such as $Yb^{3+}$, $Sc^{3+}$, or $Y^{3+}$, the rare-earth-doped $SrCeO_3$ becomes a p-type semiconductor if the atmosphere is free from hydrogen or water vapor. Cerium in cerates exists as a tetravalent state with an ionic radius of 0.1010 nm (CN = 6[26]), which is in the radius range of heavier rare earths. Consequently, the suitable candidates for the dopant are trivalent rare earths whose ionic radius is close to the size of $Ce^{4+}$ such as $Yb^{3+}$, $Y^{3+}$, etc. Proton conduction appears when the cerates are heated at several hundred degrees centigrade in $H_2$

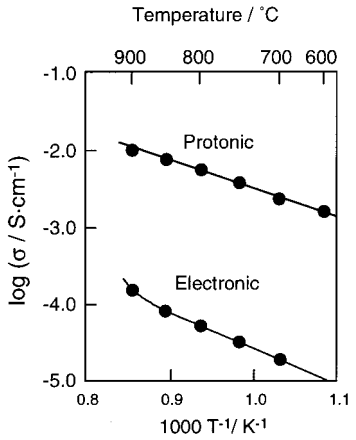


**Figure 6.** Comparison of the conductivity difference between protonic and electronic conductivity of $SrCe_{0.95}Yb_{0.05}O_{3-x}$ in hydrogen atmosphere. (Reprinted with permission from ref 27. Copyright 1995 Elsevier Science B.V.)

or humid atmosphere. Figure 6 compares the conductivity difference between protonic and electronic conductivity of $SrCe_{0.95}Yb_{0.05}O_{3-x}$ in a hydrogen atmosphere.[27] The electronic conductivity is approximately 2 orders of magnitude lower than that of the proton conductivity. Figure 7 presents the conductiv-

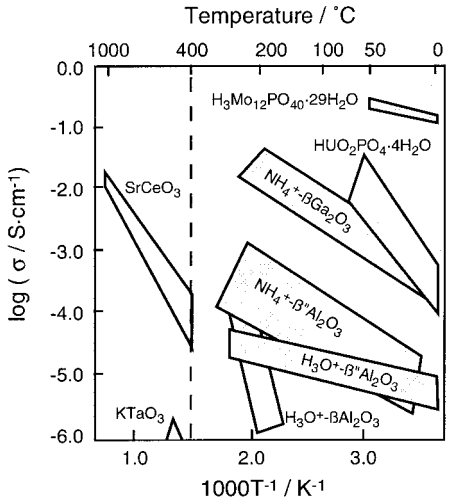


**Figure 7.** Conductivity vs 1/*T* relationship of representative protonic conductors. (Reprinted with permission from ref 27. Copyright 1995 Elsevier Science B.V.)

ity vs 1/*T* relationship of representative protonic conductors in comparison with $SrCeO_3$. Most proton conductors are not stable at temperatures higher than 400 °C, except for cerates and $KTaO_3$. For applications at higher temperatures, the cerates are expected to be useful since the conductivity of $KTaO_3$ is considerably lower. Among the rare-earth-substituted cerates, Yb shows the highest proton conductivity at $Yb^{3+}$ concentration of 5 mol % due to the fact that the ionic radius of $Yb^{3+}$ (0.1008 nm; CN = 6[26]) is the same as that of $Ce^{4+}$ (0.1008 nm; CN = 6[26]).

Figure 8 depicts a three-dimensional schematic illustration of the total and the proton conductivity as functions of $O_2$ and $H_2O$ partial pressures. The proton transference number enhances with the in-

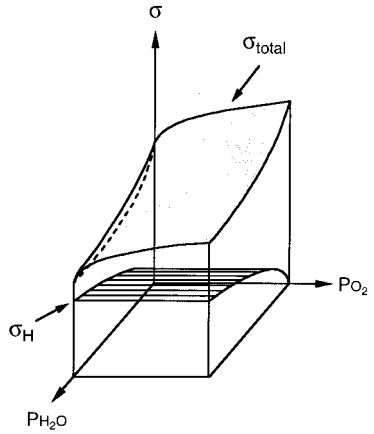


**Figure 8.** Three-dimensional illustration of the total and the proton conductivity. (Reprinted with permission from ref 28. Copyright 1983 Elsevier Science B.V.)

crease in water vapor pressure, as shown by its trace in the $pH_2O$ plane, while the total conductivity decreases. The number of holes formed by Yb doping in $SrCeO_3$ decreases in a humid atmosphere to produce proton and lowers the total conductivity but enhances the proton transference number, thus explaining the observed behavior. Cerates become proton conductors after hydrogen enters the cerate crystal lattice.[28] The hydrogen solubility in SrCe(Yb)-$O_3$ solid electrolyte is directly revealed by the proton conducting characteristics of the cerate solid electrolyte. The hydrogen solubility of $SrCe(Yb)O_3$ is compared with those of other oxides in Figure 9. SrCe-

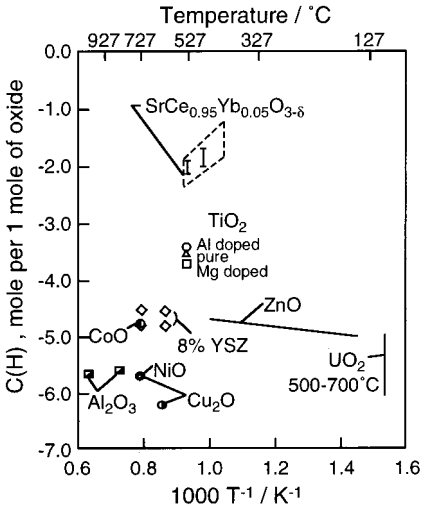


**Figure 9.** Hydrogen solubility on $SrCe(Yb)O_3$ compared with those of other oxides. (Reprinted with permission from ref 27. Copyright 1995 Elsevier Science B.V.)

$(Yb)O_3$ was found to show a high hydrogen solubility, and this directly results in the high proton conducting behaviors in this compound.

First-principles MD simulations were conducted for Y-doped $SrCeO_3$ and the microscopic mechanism of the proton migration extracted from the stable $H^+$ positions, probable proton conduction paths, and the doped acceptor effects. Figure 10 shows the stable ionic configurations near the proton in Y-doped $SrCeO_3$. Small white, black, large gray, and large white circles are the positions of the proton, $O^{2-}$,

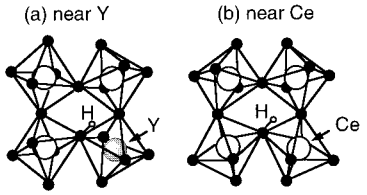


**Figure 10.** Stable ionic configurations near proton in Y-doped $SrCeO_3$. Small white, medium black, large gray, and large white balls indicate the positions of proton, $O^{2-}$, and doped acceptor, in this case, $Y^{3+}$ and $Ce^{4+}$, respectively. (Reprinted with permission from ref 29. Copyright 1998 Elsevier Science B.V.)

doped acceptor (in this case, $Y^{3+}$), and $Ce^{4+}$, respectively. It becomes clear that the proton exists as an O−H bond state and the frequency of the stretching vibration in O−H bonds is dependent on the position of the proton in the crystal. Proton motion is expected to diffuse in one of the following ways: proton diffuses around the $O^{2-}$ ion to which it is bound while retaining the O−H bond length of about 0.1 nm; the proton diffuses between neighboring $O^{2-}$ ions by switching the O−H bond in one octahedron; the proton can diffuse between two $O^{2-}$ ions which belong to different octahedra.[29,30]

The proton conducting pathway was investigated by QENS (quasi-elastic neutron scattering) experiments on $Sr\,Ce_{0.95}Yb_{0.05}H_{0.02}O_{2.985}$ and is summarized in Figure 11. Proton starts in the trapped state

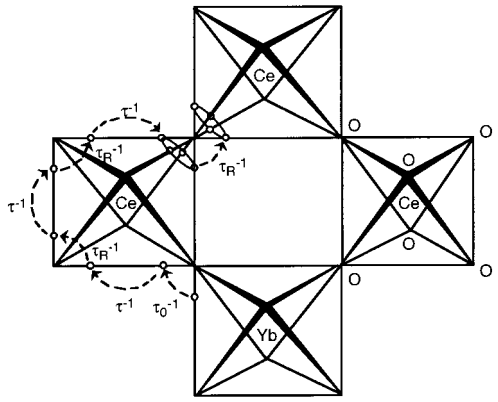


**Figure 11.** Proton conduction pathway investigated by QENS experiments on $SrCe_{0.95}Yb_{0.05}H_{0.02}O_{2.985}$. (Reprinted with permission from ref 31. Copyright 1996 OPA Amsterdam B.V. Publishers.)

bonded to a dopant ion of $Yb^{3+}$ and manages to migrate into the free state by jumping from $O^{2-}$ ion to $O^{2-}$ ion.[31]

**b. Proton Conductors with New Types of Perovskite.** In the course of exploring new types of proton conductors with the perovskite-type structure, the off-stoichiometric complex was found as a suitable candidate. The compounds are categorized as a new complex or a mixed type and expressed as $A_2B'B''O_6$ and $A_3B'B''_2O_9$. In the case of $A_2B'B''O_6$, A, B′, and B″ represent divalent ($Sr^{2+}$ or $Ba^{2+}$), trivalent, and pentavalent cations, respectively. The mean valency on the B site is 4+ when $A_2B'B''O_6$ compound is in a stoichiometric state. Oxygen vacancies can be produced simply by changing the stoichiometry with an increase in B′ content and a decrease in B″ content. An example is $Sr_2(Sc_{1+x}Nb_{1-x})O_{6-x}$ ($x = 0.05$ and 0.1). The proton conductivity of the simple perovskite $Sr_2(Sc_{1+x}Nb_{1-x})O_{6-x}$ ($x = 0.05$ and 0.1) is in the $M^{3+}$-doped $SrCeO_3$ and $BaCeO_3$ region. Since the compound does not contain Ce, ionic conducting behavior is predominant even in a severe reducing atmosphere such as $CO/CO_2$.[32] In this case, a p-type conduction appears at an oxygen pressure higher than $10^4$ Pa, showing one of the typical features of the perovskite structure dependence of conduction mechanism on oxygen partial pressures.

For $A_3B'B''_2O_9$, B′ is in the divalent state while A and B″ have the same valency of 2+ and 5+, respectively. In the off-stoichiometric $Ba_3(Ca_{1.18}Nb_{1.82})O_{9-x}$, the conductivity exceeds that of Nd-doped $BaCeO_3$ while maintaining a similar activation energy. Since the valence states of A, B′, and B″ are neither trivalent nor tetravalent, which rare earths generally possess, $A_3B'B''_2O_9$ cannot be grouped as solid electrolytes with rare earths. These off-stoichiometric solid electrolytes are still stable after exposure to a reducing atmosphere of $CO/CO_2$, while well-known proton conductors of the cerate series can be easily reduced by the valence change of $Ce^{4+}$ to the lower valent state.

**c. Brownmillerite- and Pyrochlore-Type Proton Conductors.** The compounds of $Ba_2GdIn_{1-x}Ga_xO_5$ ($x = 0$, 0.2, 0.4) have a conductivity up to $5 \times 10^{-3}$ $S\cdot cm^{-1}$ at 600 °C and show relatively low activation energies supporting the premise that solid electrolytes with brownmillerite structure are promising materials for achieving high ionic conductivity.[33] From their measurements, authors speculate that the brownmillerite solid electrolyte is a protonic conductor. However, it is not definitely determined whether the conducting species is proton or oxide yet.

Pyrochlore-type $Ln_2Zr_{2-x}Y_xO_{7-a}$ (L = La, Nd, Sm, Gd, and Er) have also been demonstrated to be protonic conductors. In this case also, replacing the tetravalent Zr with trivalent rare earths produces oxide vacancies which are essential for the proton conduction in the solid.[34]

### *3. Divalent Cation Conductors*

**a. $\beta$- and $\beta''$-Alumina-Type Divalent Cation Conductors.** $\beta$-Alumina with general composition $Na_{1+x}Al_{11}O_{17+x/2}$ ($0.2 \leq x \leq 0.7$) was discovered in 1967.[6] $Na^+-\beta$-$Al_2O_3$ has a layered structure with a conducting NaO plane sandwiched between $Al_{11}O_{16}$ layers. The $Na^+-\beta''$-$Al_2O_3$, whose composition is generally expressed as $Na_{1+x}M_xAl_{11-x}O_{17}$ (M = divalent cation), also has a similar structure with a $Na_2O$ plane and a $MgAl_2O_4$ layer. The difference between these two representative alumina structures is the atomic arrangement within the layers. Three crystallographically nonequivalent sites exist for $Na^+$ cations in the conduction planes of $Na^+-\beta$-$Al_2O_3$ (the nine-coordinated Beevers−Ross-type position (BR), the five-coordinated anti-Beevers−Ross-type position (aBR), and the eight-coordinated mid-oxygen site (mO)). At room temperature, $Na^+$ ions occupy the BR sites, and $Na^+$ ions are distributed statistically between the three sites at elevated temperatures. On the other hand, $Na^+-\beta''$-$Al_2O_3$ has only two sites which are eight-coordinated mO and seven-coordinated BR sites.

Due to the fast diffusion properties of the cations in the conduction planes, the sodium ions can be easily replaced by another mono-, di-, or trivalent cation by a simple ion exchange reaction method. Generally the ion exchange occurs much faster in $\beta''$-alumina than $\beta$-alumina and in single crystals than in polycrystals. A divalent rare-earth-containing $Eu^{2+}$–$\beta''$-alumina single crystal was also prepared. The ion exchange was carried out with $EuCl_2$ in an evacuated quartz tube in order to preserve the oxidation state of Eu(II) (in the case of $Eu^{3+}$, the atmosphere in the quartz tube was filled with $Cl_2$). The exchange was greater than 99%, and the conductivity of $Eu^{2+}$–$\beta''$-alumina was $4.7 \times 10^{-2}$ S·cm$^{-1}$ at 400 °C. The conductivity and activation energy of the $Eu^{2+}$–$\beta''$-alumina are almost equal to other divalent $\beta''$-alumina. While the exchange was almost complete (also greater than 99%) in the case of $Eu^{3+}$ exchange, meaningful conductivity data were not obtained. The conductivity value must be biased low, and we must treat the data with caution because of residual $Na^+$ ion migration in the single crystal.[35]

$Eu^{2+}$–$\beta''$-alumina in polycrystalline form was later prepared by the same ion exchange method.[36] Figure 12 shows the temperature dependence of the electrical conductivity for the $Eu^{2+}$-polycrystalline $\beta''$-alumina and the single-crystal $\beta''$-alumina. The ion exchange ratio reached 99.5%, and the conductivity is $5.0 \times 10^{-3}$ S·cm$^{-1}$ at 400 °C, which is 1 order of magnitude lower than that of the single crystal. However, the conductivity of exchanged $\beta''$-$Al_2O_3$ was independent of the exchange ratio, and the reason is not clear yet.

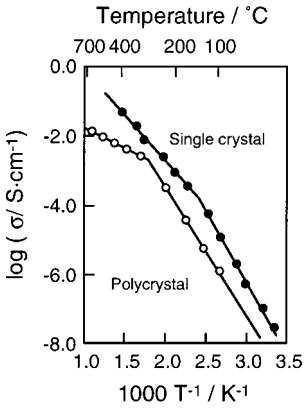


**Figure 12.** Temperature dependence of electrical conductivity for the $Eu^{2+}$-polycrystalline $\beta''$-alumina and single-crystal $\beta''$-alumina. (Reprinted with permission from ref 36. Copyright 1990 Elsevier Science Publishers B.V.)

In addition, despite the presence of $Eu^{2+}$ ions in the $\beta''$-alumina, the conducting species was not identified neither in $Eu^{2+}$–$\beta''$-$Al_2O_3$ single crystal nor in the polycrystalline form and the residual $Na^+$ cation contribution must be still taken into account. In the case of $\beta$-alumina single crystals, a satisfactory exchange ratio was not obtained because the ion diffusion rate is very low.[37] For polycrystals with $\beta$-alumina structure, the ion exchange is even more difficult to proceed and the ion conducting characterization cannot be done satisfactorily at all. Some of the expected applications of these $\beta$- and $\beta''$-$Al_2O_3$ phases are for novel phosphors and laser hosts.

**b. $YPO_4$–$M_{1.5}PO_4$ (M = Ca, Mg).** For the $YPO_4$-based samples with a mixture of $Mg_{1.5}PO_4$ and $Ca_{1.5}PO_4$,[25] the maximum values of conductivity of $5.0 \times 10^{-5}$ and $1.2 \times 10^{-3}$ S·cm$^{-1}$ were obtained, respectively, as shown in Figure 13.[25] The $Ca^{2+}$ ion conductivity is 3 orders of magnitude higher compared with that of pure divalent $Ca^{2+}$ ion conducting CaS.

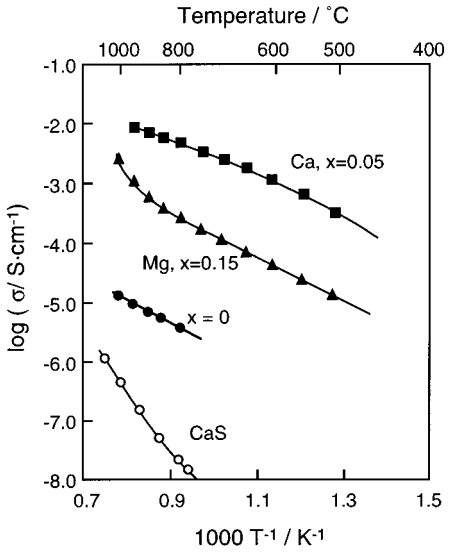


**Figure 13.** Temperature dependencies of the electrical conductivity for $(YPO_4)_{1-x}(M_{1.5}PO_4)_x$ (M = Ca, Mg) with the data of CaS. (Reprinted with permission from ref 25. Copyright 1989 Elsevier Science Publishers B.V.)

## B. Anionic Conductors

### *1. Chloride Ion Conductors*

Most chlorides are soluble in water, and they cannot be applied as practical solid electrolytes. For the purpose of developing $Cl^-$ anion conductors which are suitable for practical applications, only materials which contain $Cl^-$ anion and are water insoluble are possible candidates, and here, rare-earth oxychlorides were selected. Among rare-earth oxychlorides, lanthanum oxychloride shows the highest stability at elevated temperatures. However, the conductivity of LaOCl is very low. A route to enhance the conductivity is to dope a lower valent cation, compared with trivalent $La^{3+}$, at the La site to create $Cl^-$ vacancies. For that purpose, $Ca^{2+}$ was doped in the trivalent La site of LaOCl and ion conducting behavior was characterized.[38] By the doping of 1.6 mol % Ca in the La site, the conductivities enhanced by 1 order of magnitude in comparison to that of pure LaOCl. For the compensation of charge neutrality, anion vacancies of $Cl^-$ or $O^{2-}$ should be created. To clarify which vacant species is formed, polarization measurements were carried out in $O_2$, $N_2$, and 1 vol % $Cl_2$ in nitrogen atmosphere. A clear polarizing behavior was similarly observed in both $O_2$ and $N_2$, while no such a polarization was recognized in 1 vol % $Cl_2$ in nitrogen. This result clearly indicates the fact that by polarization measurement with applying dc current, $Cl^-$ anion was continuously supplied at the cathode and conducts inside the oxychloride bulk through the $Cl^-$ vacancies and moves to the anode and is released as

$Cl_2$ gas. This proves that the conducting anion is $Cl^-$. The $Cl^-$ anion transference number is estimated to be higher than 0.9.

### 2. Oxide Ion Conductors

**a. Cerium Oxides.** Cerium oxide, ceria, has a fluorite structure and exhibits oxide anion conducting behavior. The conductivity of pure cerium oxide is low due to a lack of oxide anion vacancies. Therefore, the substitution of tetravalent Ce by a lower valent cation is a method of enhancing the oxide ionic conductivity. One of the appropriate dopant candidates is a rare-earth cation which has a stable trivalent state.

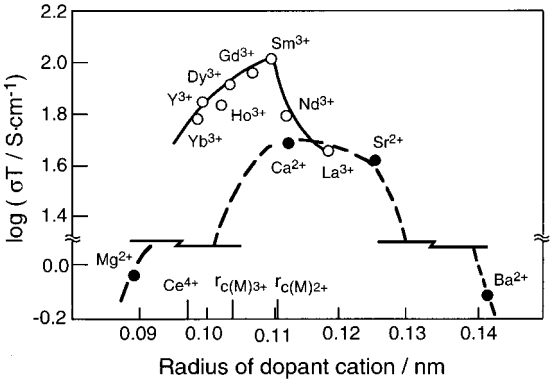


**Figure 14.** Dopant ionic radius dependencies of the oxide ionic conductivity of doped ceria at 800 °C. (Reprinted with permission from ref 39. Copyright 1996 Elsevier Science B.V.)

Figure 14 depicts the dopant ionic radius dependencies of the oxide ionic conductivity of doped ceria at 800 °C.[39] In the series of rare-earth-doped $CeO_2$, the highest conductivity was obtained for the solid solution with $Sm^{3+}$ doping. The conductivity of $Ce_{1-x}Gd_xO_{2-x/2}$ at 700 °C, which shows the second highest ion conductivity, is almost equivalent to that of stabilized zirconia at 1000 °C.[40] Among the alkaline-earth series, the doping of $Ca^{2+}$ is most effective in enhancing the conductivity because its ionic radius is close to that of $Sm^{3+}$.

Figure 15 presents the domain which behaves predominantly as a pure oxide anion conductor with fluorite structure.[39] As can be seen from the figure, thoria- (YDT) and zirconia-based oxides (CSZ) are still in the range of pure solid electrolyte domain even at low oxygen pressures. In contrast, doped $Bi_2O_3$ and $CeO_2$ have a small electrolyte domain at the same low oxygen pressures. One of the crucial disadvantages of cerium oxide from a practical application point of view is that electronic conduction appears at relatively low oxygen pressures and the oxide ionic transference number decreases to 0.5 in the atmosphere where $pO_2$ is equal to ca. $10^{-8}$ Pa (1000 °C). In the rare-earth oxide-doped ceria, $Sm_2O_3$-doped ceria is the most stable against reduction.

The hydrothermal syntheses of $Ce_{1-x}Sm_xO_{2-x/2}$ and $Ce_{1-x}Ca_xO_{2-x}$ solid solutions were successfully carried out temperatures as low as 260 °C in less than 2 h and the properties were systematically investigated.[41] The particles obtained were ultrafine crystallites with dimensions of 40−68 nm. Since the particle

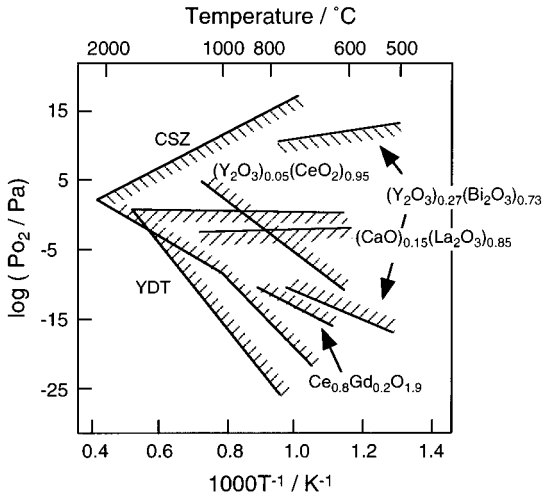


**Figure 15.** Domain which behaves predominantly as a pure oxide anion conductor with fluorite structure. (Reprinted with permission from ref 39. Copyright 1996 Elsevier Science B.V.)

size is small enough, the sintering of the solid solutions can be carried out even at 1400 °C, which is about 200 °C lower than the typical temperature of the solid-state reaction method. Furthermore, $(Ce_{0.83}Sm_{0.17})_{1-x}Ln_xO_{2-y}$(Ln = Pr, Tb) was also prepared by the same hydrothermal synthesis method at 260 °C.[42] From transmission electron microscopy (TEM) observation, the average crystallite size was in the range between 10 and 60 nm. The doping of Pr or Tb was attempted to investigate the electrolytic domain boundary (EDB) of Sm-doped ceria and clarified that neither Pr nor Tb doping shows a significant effect on the EDB of Sm-doped ceria. However, this result is not consistent with their preliminary results,[43] and thus, the effects of Pr- or Tb-doping do not appear to be well understood yet.

**b. Perovskite-Type Structures.** While $LaYO_3$ ($T_{mp}$ = 1800 °C) and $LaAlO_3$ ($T_{mp}$ = 2110 °C), both show a p-type conduction at high oxygen pressures, they have been reported to be oxide ionic conductors.[44,45] These perovskite-type solid electrolytes are stable at low oxygen pressure and are useful for measurement of the Gibbs energy change of the overall cell reaction using a metal and metal oxide mixture.[44] However, the conductivity is still low. Recently it was clarified that by doping Ca in the La site, the conductivity is enhanced by more than 2 orders of magnitude, and at a high oxygen pressure region such as air, p-type conduction appears and the perovskite compound shows a mixed conductor of oxide anion and hole species. The Ca- and Ga-co-doping into $NdAlO_3$ enhances the oxide ion conductivity comparable to the electrical conductivity of stabilized zirconia.[46] As clearly indicated as a common feature of the perovskite-type in this review, the Ca- and Ga-co-doped $NdAlO_3$ system also becomes a p-type semiconductor at oxygen pressures higher than $10^4$ Pa. This boundary ($pO_2 = 10^4$ Pa) is identical for the perovskite-type ion conductor series with migrating ion species both for proton and oxide ions.

The word "free" volume is defined as the difference between the perovskite unit cell volume and the volume occupied by the constituent ions in the lattice.

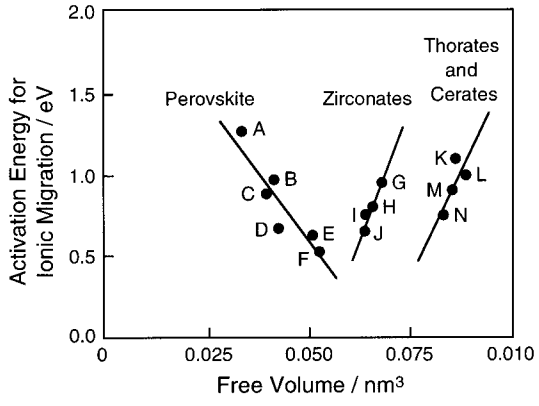


| | | | | | |
|---|---|---|---|---|---|
| A. | $CaTi_{0.7}Al_{0.3}O_3$ | $O^{2-}$ | H. | $Zr_{0.84}Y_{0.16}O_{1.84}$ | $O^{2-}$ |
| B. | $CaHf_{0.95}Yb_{0.05}O_3$ | proton | I. | $Zr_{0.85}Yb_{0.15}O_{1.85}$ | $O^{2-}$ |
| C. | $BaZr_{0.95}Yb_{0.05}O_3$ | proton | J. | $Zr_{0.82}Sc_{0.18}O_{1.82}$ | $O^{2-}$ |
| D. | $SrCe_{0.95}Yb_{0.05}O_3$ | proton | K. | $Th_{0.95}Ca_{0.05}O_{1.95}$ | $O^{2-}$ |
| E. | $BaCe_{0.9}Gd_{0.1}O_3$ | $O^{2-}$ | L. | $Th_{0.85}Ca_{0.15}O_{1.85}$ | $O^{2-}$ |
| F. | $BaCe_{0.95}Nd_{0.05}O_3$ | proton | M. | $Ce_{0.8}La_{0.2}O_{1.8}$ | $O^{2-}$ |
| G. | $Zr_{0.82}Sm_{0.18}O_{1.82}$ | $O^{2-}$ | N. | $Ce_{0.85}Ca_{0.15}O_{1.85}$ | $O^{2-}$ |

**Figure 16.** Correlations between $\Delta E$ for $O^{2-}$ transport and free volume for perovskite-type solid. (Reprinted with permission from ref 47. Copyright 1991 Elsevier Science Publishers B.V.)

This free volume has been found to be applicable for both perovskite and fluorite phase solid solutions. Figure 16 shows the correlations between activation energy for ionic migration ($\Delta E$) for $O^{2-}$ transport and the free volume for a perovskite-type solid. As can be seen in Figure 16, the relation can be extended for zirconates, cerates, and thorates. Since both $O^{2-}$ and $OH^-$ ions (proton conduction appears through $OH^-$) transport through the perovskite lattice, a linear trend is observed. Linear although opposite relations were observed in Figure 16; free volume would be an appropriate screening parameter. From a free volume point of view, the optimum value is 0.03−0.035 $nm^3$ for perovskites.[47]

In a similar manner, $BaCe_{0.9}Bi_{0.1}O_{3-x}$ and $BaTh_{0.95}La_{0.1}O_{3-x}$ have been studied, and both oxides were found to show an oxide ion conducting behavior. However, these compounds are unstable and reproducible data could not be obtained.[45]

During the course of attempting to enhance the oxide anion conductivity with the perovskite-type structure, attention was focused on $LaGaO_3$ and it was found that the doping of Sr on the La site and Mg on the Ga site greatly enhances the oxide ionic conductivity of $LaGaO_3$. Figure 17 depicts the comparison of oxide ionic conductivity with some well-known oxide ionic conductors.[48] The oxide ionic conductivity of La−Sr−Ga−Mg−O exceeds the value of Sc-doped $ZrO_2$ (SSZ) and is between the value of $ZrO_2$−$Sc_2O_3$ and $Bi_2O_3$−$Y_2O_3$. The $LaGaO_3$-based solid electrolyte maintains pure oxide ionic conducting characteristics over a wide range of oxygen pressures, ranging from $10^5$ to $10^{-16}$ Pa, and over a wide temperature range from 500 to 1000 °C.[49] In the case of $CeO_2$- and $Bi_2O_3$-based oxides, n-type semiconduction becomes predominant under a low oxygen pressure region, and especially for the $Bi_2O_3$-based oxides, thermal stability is not satisfactory at all. In contrast, $LaGaO_3$ co-doped with Sr and Mg possesses such high thermal durability, as mentioned

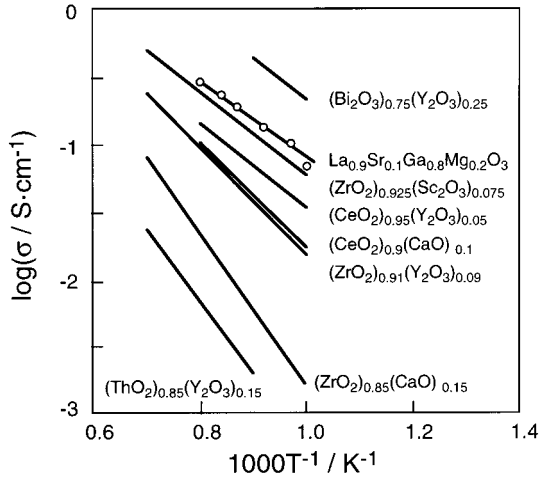


**Figure 17.** Comparison of oxide ionic conductivity with some well-known oxide ionic conductors. (Reprinted with permission from ref 48. Copyright 1994 American Chemical Society.)

above, and is expected to be a promising new oxide ionic conductor. One of main targets is to apply this as a component of solid oxide fuel cells (SOFCs).[50]

Another perovskite oxide, barium terbium oxide ($BaTbO_3$) doped with 10 mol % indium at the Tb site, shows an ionic transference number of 0.87 at 600 °C. This perovskite solid electrolyte was reported to have some potential application at intermediate temperatures such as the operation temperatures of SOFCs.[51]

**c. Lanthanum Molybdates.** The $La_2Mo_2O_9$ solid shows a phase transition at approximately 580 °C which is accompanied by an enhancement of the oxide ion conductivity of about 2 orders of magnitude. Above this temperature, the molybdate becomes a good oxide anion conductor and reaches a conductivity of $6 \times 10^{-2}$ $S \cdot cm^{-1}$ at 800 °C as shown in Figure 18. $La_2Mo_2O_9$ can be also described as $La_2Mo_2O_{8+1}\square$,

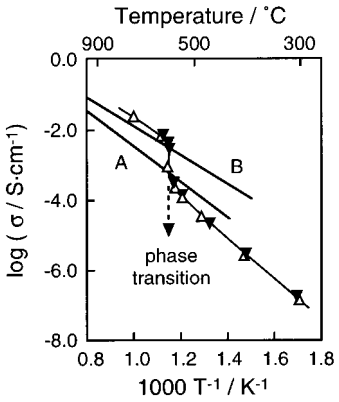


**Figure 18.** Temperature dependencies of oxide anion conducting $La_2Mo_2O_9$. Lines A and B represent the conductivities of $0.87(ZrO_2)$−$0.13(CaO)$ and $0.9(ZrO_2)$−$0.1(Y_2O_3)$, respectively. (Reprinted with permission from Nature (http://www.nature.com), ref 52. Copyright 2000 Macmillan Publishers.)

and through the vacancies (□), oxide anions can migrate. The electronic conductivity is estimated to be less than 1%, and also the molybdate is reported to show a high stability even in an atmosphere of 5 Pa of air (1 Pa $O_2$) at 650 °C.[52]

The crystal structure of the fast oxide ion conducting $La_2Mo_2O_9$ phase has been already clarified by ab initio using X-ray and neutron powder diffraction patterns.[53] The details are given by Goutenoire et al. However, as can be easily speculated, the compounds with Mo as a constituent element are easily reduced, especially in contact with metals, which leaves some critical problems still to be overcome.

**d. Lanthanoid Oxyfluorides.** By the reaction between oxide and fluoride of single rare-earth series, single rare-earth metal oxyfluorides were prepared as in the chemical reaction described below.

$$Ln_2O_3 + LnF_3 \rightarrow 3LnOF \quad (1)$$

$$Ln_2O_3 + 2LnF_3 \rightarrow Ln_4O_3F_6 \quad (2)$$

When the reaction is carried out with Ln oxide and Ln′ fluoride, where Ln and Ln′ indicate different rare-earth species, the binary rare-earth oxyfluorides of $Ln_2Ln'O_3F_3$ and $Ln_2Ln'_2O_3F_6$ were prepared as shown in eqs 3 and 4.

$$Ln_2O_3 + Ln'F_3 \rightarrow Ln_2Ln'O_3F_3 \quad (3)$$

$$Ln_2O_3 + 2Ln'F_3 \rightarrow Ln_2Ln'_2O_3F_6 \quad (4)$$

$Ln_2Ln'_2O_3F_6$, in which Ln and Ln′ are different rare earths, are the oxide anion conducting solid electrolytes showing a much higher ion conductivity compared with that of yttria-stabilized zirconia (YSZ) as presented in Figure 19.

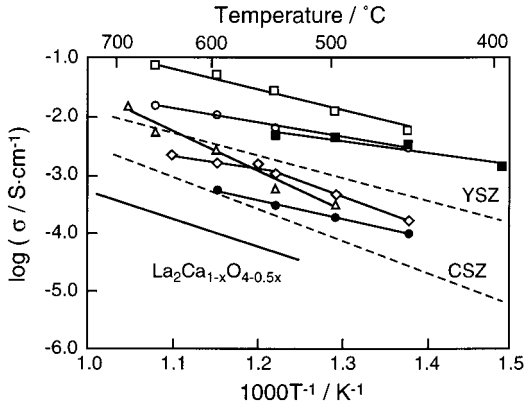


**Figure 19.** Temperature dependencies of oxide anion conducting $Ln_2Ln'_2O_3F_6$ in which Ln and Ln′ are different rare earths (□, $Nd_2Eu_2O_3F_6$; ○, $Nd_2Sm_2O_3F_6$; ■, $La_2Eu_2O_3F_6$; △, $Nd_2Y_2O_3F_6$; ◇, $Nd_2Gd_2O_3F_6$; ●, $Nd_2Ce_2O_3F_6$) with those of representative oxide anion conductors. (Reprinted with permission from ref 58. Copyright 2000 Elsevier Science S.A.)

The conductivities of $Nd_2R'_2O_3F_6$ (R′ = Y, Sm, Eu, and Gd) are higher than those of YSZ. Among the $R_2R'_2O_3F_6$ series, $Nd_2Eu_2O_3F_6$ shows the highest oxide anion conductivity. In particular, the conductivity of $Nd_2Eu_2O_3F_6$ at 650 °C reaches $5.0 \times 10^{-2}$ S·cm$^{-1}$, and this value is close to the conductivity of $(ZrO_2)_{0.89}(Y_2O_3)_{0.11}$ (YSZ-11) at 900 °C. $Nd_2Eu_2O_3F_6$ is an oxide anion conducting solid electrolyte, and the oxide anion transference number is higher than 0.9 at 500−700 °C (fluoride ion conduction was denied by the electrolysis measurement[54]). From a dc polarization method, the electron transference number is estimated to be smaller than 0.05. The preparation process of the oxyfluorides should be carried out in a dry atmosphere. For example, $Nd_2Eu_2O_3F_6$ is synthesized from 1:2 $Nd_2O_3$:$EuF_3$. $Nd_2Gd_2O_3F_6$ was also prepared. $Nd_2Gd_2O_3F_6$ was stable up to approximately 650 °C, a temperature 50 °C below the stability temperature of $Nd_2Eu_2O_3F_6$. By comparing the oxide ion conductivity, $Nd_2Gd_2O_3F_6$ shows lower conductivity than $Nd_2Eu_2O_3F_6$.[55]

Once prepared, the oxyfluoride compounds are chemically stable up to ca. 600 °C even in a humid atmosphere. However, pyrohydrolysis starts at around 700 °C, and rare-earth oxyfluorides are easily hydrolyzed at temperatures higher than 800 °C.[56]

The oxyfluoride series has demonstrated a unique character of unusually high $O^{2-}$ ion conductivity which exceeds stabilized zirconias, and $Nd_2Eu_2O_3F_6$ is reported to be a suitable oxide anion conducting solid electrolyte candidate for oxygen sensors and a fuel cell component applicable at a relatively moderate temperature of 450 °C. Despite these positive contributes, the compounds are still not promising due to their low stability at elevated temperatures where they function as solid electrolytes. Consequently, the temperature field of application is very limited.

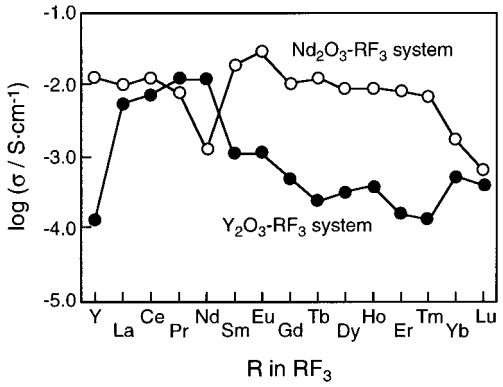


**Figure 20.** Relationship between the conductivity at 650 °C and various R for $R_2Y_2O_3F_6$ and $Nd_2R'_2O_3F_6$. (Reprinted with permission from ref 58. Copyright 2000 Elsevier Science S.A.)

Figure 20 presents the relationship between conductivity and various R and R′ for the $R_2Y_2O_3F_6$ and $Nd_2R'_2O_3F_6$ systems. Most of the neodymium oxyfluorides show conductivities as high as $10^{-2}$ S·cm$^{-1}$ ($\log \sigma = -2$).

In the case of $Nd_2R'_2O_3F_6$, conductivity higher than $10^{-2}$ S·cm$^{-1}$ was obtained for R = Y, Sm−Er. The conductivity reduces gradually with the increase in atomic number from Eu to Lu. An ionic transference number of higher than 0.75 was observed, except for two compounds containing Ce or Tb. From the oxygen pump method, the charge carrier was identified to be mainly oxide anion. Therefore, the fluoride anion transference number is estimated to be less than 0.01. The conductivity of $Nd_2Y_2O_3F_6$ is $8.0 \times 10^{-2}$ S·cm$^{-1}$ at 750 °C, and this value is comparable to that of yttria-stabilized zirconia (YSZ-11) at 1100 °C. The transference number of higher than 0.75 is still

insufficient for practical application. In reality, a transference number higher than 0.99 is required.

In the case of the simple oxyfluoride $Nd_2Nd_2O_3F_6$, the conductivity decreases appreciably, which may be due to the impossibility of the formation of a special arrangement of anions in the crystal to produce an easy pathway for oxide anions. However, the stability of solid electrolytes based on oxyfluorides is questionable, especially for applications such as rechargeable batteries and fuel cell components.[57]

The high-temperature cubic $ZrO_2$ phase can be stabilized by using rare-earth fluorides as additives at temperatures around 1100 °C. This rare-earth fluoride-stabilized zirconia (LnFSZ) also shows oxide anion conducting characteristics. While the oxide anion transference number is greater than 0.9 even at 450 °C, the conductivity is smaller than that of YSZ.[54,58]

**e. Lanthanum Oxides.** Lanthanum oxide ($La_2O_3$) doped with SrO or CaO with a hexagonal structure shows an oxide anion conducting behavior. The aliovalent cation doping creates oxygen vacancies, and they act as charge carriers at elevated temperatures. The bulk oxide anion conductivity of $La_2O_3$ doped with SrO or CaO is similar to that of similarly doped $ZrO_2$. In addition, the solid solutions are predominantly ionic conductors in a wide oxygen pressure region (from $10^{-3}$ to $10^{-20}$ Pa).[59]

**f. Brownmillerite- and Pyrochlore-Type Structures.** Among the perovskite-related $A_2B_2O_5$ lattice in which oxygen vacancies appear (1/6 of the oxygen atoms are removed in the unit cell) and which corresponds to the brownmillerite structure, $Sr_2Gd_2O_5$ and $Sr_2Dy_2O_5$ have conductivities of $2 \times 10^{-2}$ and $3.65 \times 10^{-2}$ S·cm$^{-1}$ at 600 °C, respectively. A high population of anion vacancies is presented in the lattice and explains the high oxide ion conductivity.[60]

A new single-phase compound of $Ba_3In_2CeO_8$ has been prepared by including Ce in $Ba_2In_2O_5$, which crystallizes in the Brownmillerite structure at room temperature. Since $Ce^{4+}$ is randomly distributed while introducing oxygen vacancies, this results in a significant increase in conductivity in the temperature region from 100 to 450 °C, which is remarkably higher than that obtained for Gd-doped $CeO_2$ and Y-doped $ZrO_2$. The ionic transference number of $Ba_3In_2CeO_8$ reaches 0.94 at 500 °C.[61]

The system of $Y_2O_3-TiO_2$ was investigated and reported to structurally change from fluorite-type to pyrochlore-type with the $TiO_2$ amount higher than ca. 55 mol %.[62] While the conductivity of the pyrochlore phase is higher than that of fluorite one, the conductivity increases at oxygen pressures below ca. $10^{-13}$ Pa, depending on the operating temperature, as well as at pressures higher than $10^5$ Pa. Even if the stability of $Y_2Ti_2O_7$ is in a satisfactory temperature region, application of this oxide ion conductor is limited only in the intermediate oxygen pressure region. Another $Sm_2Zr_2O_7$ pyrochlore phase was also prepared. However, the oxygen pressure dependencies are similar.[63] The stoichiometric pyrochlore phase of $Gd_2Zr_2O_7$ was reported to be another candidate for an oxide ion conductor.[64] The ion conductivity was still lower than that of lanthanum oxide ($La_2O_3$) doped with SrO or CaO, which is described in section II.B.2.e and is not attractive at this stage.

High oxide ion conductivity was obtained for $Gd_2(Ti_{1-x}Zr_x)_2O_7$,[65] and it was clarified that $Gd_2(Ti_{1-x}Zr_x)_2O_7$ shows a large enhancement in oxide ion conductivity as the composition changes from $Gd_2Ti_2O_7$ to $Gd_2Zr_2O_7$. This conductivity increase is estimated to be due to the structural disorder which increases the concentration of the oxygen vacancies and increases the oxide anion conductivity.[66, 67]

## *III. Solid Electrolytes with Rare Earths as Dopants*

## A. Cationic Conductors

### *1. Lithium Ion Conductors*

$Li_{1+x}Ti_{2-x}Sc_x(PO_4)_3$ was reported in 1986;[68] with the Ti site substitution for $Sc^{3+}$, the lattice size increases, since the ionic radius of $Sc^{3+}$ (0.0885 nm; CN = 6[26]) is slightly larger than that of $Ti^{4+}$ (0.0745 nm; CN = 6[26]). From this observation, it was clarified that the bottleneck size of the $Li^+$ ion migration path appreciably affects the ion conducting properties in the $LiM_2(PO_4)_3$-type structure.

In 1989, various types of rare-earth elements such as $Sc^{3+}$, $Y^{3+}$, and $La^{3+}$ were mixed with $LiTi_2(PO_4)_3$ to enhance the ion conductivity in $Li_{1+x}Ti_{2-x}R_x(PO_4)_3$ (R = Sc, Y, or La).[69] $Sc^{3+}$ ion can replace Ti, while the substitution of Ti with Y or La was not successful due to their large difference in ionic radius and results in the $LiTi_2(PO_4)_3$ and $Li_3Ln_2(PO_4)_3$ (Ln = Y or La) mixed phase. However, from the $Li^+$ ion conducting behavior, all the $LiTi_2(PO_4)_3$ solid electrolytes mixed with $Sc^{3+}$, $Y^{3+}$, or $La^{3+}$ show a considerably higher conductivity than $LiTi_2(PO_4)_3$. By rare-earth mixing with $LiTi_2(PO_4)_3$, regardless of whether they make a solid solution, the relative density (porosities of $Li_{1.3}Ti_{1.7}Sc_{0.3}(PO_4)_3$ and $LiTi_2(PO_4)_3+Li_3La_2(PO_4)_3$ mixed phase with Li:La = 1.7:0.3 are 2.0% and 0.1%, respectively) becomes appreciably higher and enhances the conductivity.[70,71]

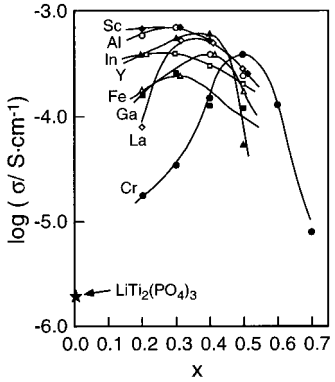


**Figure 21.** Ion conductivity change with $x$ in $Li_{1+x}M_xTi_{2-x}(PO_4)_3$ at 25 °C. (Reprinted with permission from ref 70. Copyright 1990 Electrochemical Society, Inc.)

Figure 21 shows the effect on ion conductivity with change in $x$ in $Li_{1+x}Ti_{2-x}M_x(PO_4)_3$ at 25 °C. By the $M^{3+}$ substitution, the conductivity greatly increased, and a maximum conductivity was obtained at about $x = 0.3$. In particular, $Li_{1.3}Ti_{1.7}M_{0.3}(PO_4)_3$ (M = Al or

Sc) has the highest ion conductivity of $7 \times 10^{-4}$ S·cm$^{-1}$ at 25 °C, and this value is comparable to that of $Li_3N$, which shows the highest $Li^+$ ion conductivity among $Li^+$ ion conductors as shown in Figure 22.

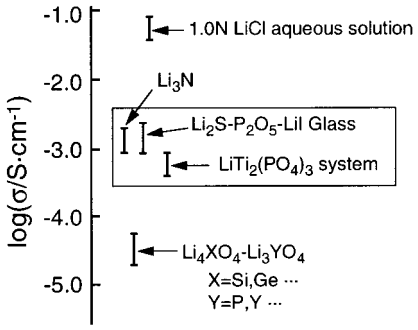


**Figure 22.** Ionic conductivity at 25 °C for the various $Li^+$ conducting solid electrolytes.

$LiLnTiO_4$ (Ln = La, Nd) were also prepared, and the lithium ion conductivity of $LiLnTiO_4$ (Ln = La, Nd) was measured. It becomes clear that $LiLaTiO_4$ shows 1 order of magnitude higher conductivity than that of $LiNdTiO_4$. However, the $Li^+$ ion conductivity of the layered perovskite $LiLnTiO_4$ (Ln = La, Nd) is much lower than that of the 3D-perovskite (Li, Ln)-$TiO_3$ series as discussed in section II.A.1.a. The high conductivity of (Li, Ln)$TiO_3$ is ascribed to the presence of $Li^+$ ions in the cubooctahedral sites along with La ions and also the existence of $Li^+$ ion vacancies. In contrast, there is no $Li^+$ ion vacancies in $LiLnTiO_4$ and the mobility of $Li^+$ ion is considerably restricted.[72]

### 2. Sodium Ion Conductors

**a. Silicate-Based Materials.** $Na_5MSi_4O_{12}$-type silicates (M = Fe, In, Sc, Y, Lu−Sm) show a comparable conductivity to that of $Na^+$−$\beta$-$Al_2O_3$ and of NASICON ($Na_3Zr_2PSi_2O_{12}$). The silicate structure is composed of $Si_{12}O_{36}$ rings which stack to form columns held apart by $MO_6$ octahedra. In $Na_5YSi_4O_{12}$, $Na^+$ ions are immobile and are situated within the rings while $Na^+$ ions between the columns easily migrate. Figure 23 depicts the log $\sigma$−$1/T$ relation for the $Na_5MSi_4O_{12}$ series. The trivalent ion which holds the largest ionic radius shows the highest conductivity and is in this case Sm. Since $Na^+$−$\beta$-$Al_2O_3$ possesses an anisotropic $Na^+$ ion conductivity, it prompted research on new high $Na^+$ ion conductors in the framework or tunnel structure where three-dimensional migration can be realized. Figure 24 presents some representative results of $Na^+$ ion conducting behaviors. At 25 °C, $Na^+$−$\beta$-$Al_2O_3$ exhibits the highest conductivity, while two silicates give a comparable conductivity to $Na^+$−$\beta$-$Al_2O_3$ at 200 °C. One of great advantages of the silicate series is that the synthesis can be completed at lower temperatures compared with that of $Na^+$−$\beta$-$Al_2O_3$, although the raw materials for silicates are more costly.[73]

**b. Sulfate-Based Materials.** Sodium sulfate has five polymorphic forms. $Na_2SO_4$-V is stable at room temperature but transforms to $Na_2SO_4$-III on heating and then finally transforms to the $Na_2SO_4$-I phase. This $Na_2SO_4$-I phase is a high $Na^+$ ion conducting

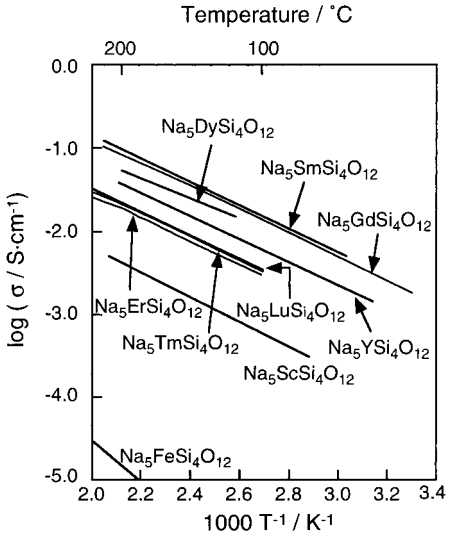


**Figure 23.** log $\sigma$ − $1/T$ relation for the $Na_5MSi_4O_{12}$ series. (Reprinted with permission from ref 73. Copyright 1978 American Chemical Society.)

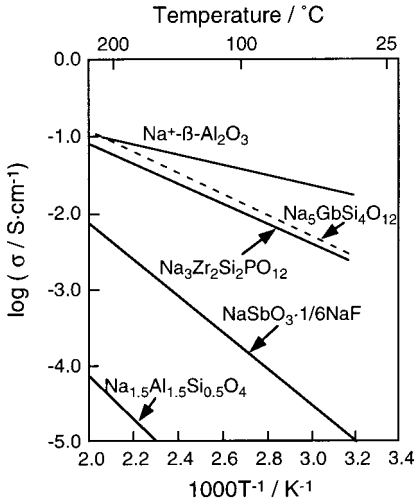


**Figure 24.** Temperature dependencies of the conductivity of the representative $Na^+$ ion conducting solids. (Reprinted with permission from ref 73. Copyright 1978 American Chemical Society.)

phase, and the sulfate functions as a solid electrolyte. In contrast, on cooling, $Na_2SO_4$-I phase makes a phase transition via the unstable $Na_2SO_4$-II phase then to $Na_2SO_4$-III phase. The $Na_2SO_4$-III phase gradually transforms to $Na_2SO_4$-V, but this transformation is sluggish and may take several months. To maintain the high $Na^+$ ion conducting $Na_2SO_4$-I phase, it is necessary to dope with aliovalent ions.

Rare-earth cations contribute greatly for that purpose. Figure 25 shows one of the representative log-($\sigma T$) vs $1/T$ relationships for sodium sulfate-based solid electrolytes. To realize the stabilization of the high-temperature $Na_2SO_4$-I phase, the rare-earth doping in $Na^+$ site has been carried out by mixing with $NaVO_3$. By this modification, $Na^+$ cation vacancies are produced and the enhancement of $Na^+$ ion conductivity is successfully achieved. By simply mixing $R_2(SO_4)_3$ (R = Eu, Pr, and Y) with $Na_2SO_4$, the conductivity also increases. However, the phase transformation from phase I to III still appears when the rare-earth-doped sulfate is cooled. Rare-earth

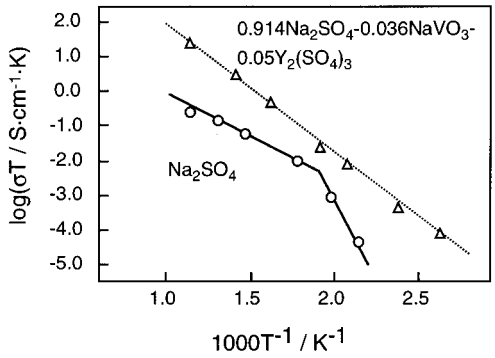


**Figure 25.** One of representative log $\sigma T$ vs $1/T$ relationship for sodium sulfate-based solid electrolytes. (Reprinted with permission from ref 74. Copyright 1984 The Chemical Society of Japan.)

sulfate mixing with sodium sulfate is therefore not sufficient for the stabilization of the high $Na^+$ ion conducting phase. Codoping of $NaVO_3$ and $R_2(SO_4)_3$ (R = Eu, Pr and Y) with $Na_2SO_4$ is considerably more effective in preserving the phase similar to the high $Na^+$ ion conductive $Na_2SO_4$-I phase.[74]

Another attempt which has been undertaken to stabilize the $Na_2SO_4$-I phase is to mix rare-earth sulfate and silicon dioxide or aluminum oxide[75,76] with $Na_2SO_4$.[77] This results in a $Na^+$ ion conductivity that is comparable to $Na_2SO_4-NaVO_3-Y_2(SO_4)_3$ and prevents the electrolyte from becoming ductile. By further additional mixing of lithium sulfate with $Na_2SO_4-Y_2(SO_4)_3-SiO_2$ solid electrolyte, the conductivity becomes approximately 320 times higher than pure sodium sulfate at 700 °C, which is within the high $Na^+$ ion conductive I phase region.[78]

### 3. Proton Conductors

Proton conduction is the charge transport mechanism in Sc (2 mol %) doped $SrTiO_3$ in a wet air atmosphere. The proton is bounded by oxide anion as if the proton shows the hydrogen bond between two oxide anions. This is expected to be responsible for the high proton conduction also in $SrTiO_3$.

The perovskite-type structure is one of famous frameworks of proton conductors. However, the perovskite structure cannot always support the proton conduction. For example, Y-doped $BaTiO_3$ does not show proton conducting behavior. For 4 mol % Sc-doped $SrTiO_3$, the conductivity in water vapor is higher than that in dry atmosphere in the temperature region below 200 °C. However, above 400 °C, conduction occurs mainly by holes or oxygen vacancies and not protons.[79] This tendency is commonly observed among perovskite-type oxide series.

$SrZrO_3$ also shows proton conducting properties at temperatures below 700 °C. At temperatures higher than 700 °C, hole conduction becomes predominant. By doping the Zr site with Y, proton conduction increases rapidly, and at $x = 0.06$, the solid solution shows the highest proton conductivity among Y-doped $SrZrO_3$ single crystals. Using the isotope effect, it has been shown that the proton conduction occurs by migration in a crystal without tunneling.[80] The conductivities of $SrTiO_3$ and $SrZrO_3$ are presented and compared in Figure 26. Also in $SrMY_{0.05}O_{2.75}$ (M = Ce or Zr) it becomes clear from isotope investigations that the proton is bound in the interstitial site between oxide anions and conducts by hopping with a thermal activation process.[81]

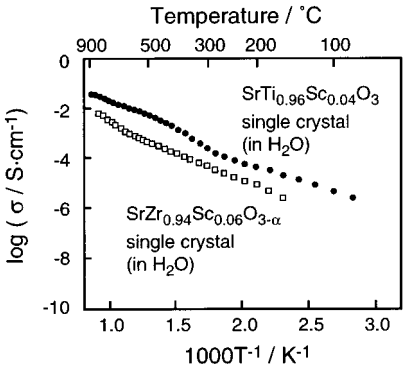


**Figure 26.** Temperature dependencies of the conductivities of Sc-doped $SrTiO_3$ and $SrZrO_3$.

The great disadvantage commonly observed for perovskite-type structures is that p-type conduction appears in a relatively high oxygen pressure and high temperature region, and this feature greatly deteriorates the applicability of the proton conductors based on the perovskite-type structure.

Perovskite-type $BaTh_{0.9}Gd_{0.1}O_3$ solid also shows proton conducting behavior. However, thorium is a low radioactive element (half-life = $1.4 \times 10^{10}$ years), and this restricts the wide application of the Th-contained-perovskite-type solid electrolyte.[82]

## B. Anionic Conductors

### 1. Zirconium Dioxides

In 1899, Nernst demonstrated oxide ion conduction in $ZrO_2-9\%Y_2O_3$.[83] Doping with 9 mol % $Y_2O_3$ is the minimum content for stabilization of the fluorite phase. The high solubility of $Y_2O_3$ in $ZrO_2$ is ascribed to the similarity between the $ZrO_2$ fluorite structure and the rare-earth oxide cubic, C-type structure.

In the case of the rare earth, La, as a dopant, the pyrochlore $La_2Zr_2O_7$ is formed due to the large ionic size of $La^{3+}$. Among the rare earths as a dopant, the most interesting dopant is $Sc^{3+}$. As the ionic radius of $Zr^{4+}$ (0.098 nm; CN = 8[26]) and $Sc^{3+}$ (0.101 nm; CN = 8[26]) are similar, only 6% is necessary to fully stabilize the fluorite phase.

In the $ZrO_2-R_2O_3$ series, the fluorite-type solid solutions have a maximum conductivity at 8−10 mol % $RO_{1.5}$ (R = Nd−Lu, Y, Sc) at compositions corresponding to near the lower fluorite phase boundary, and an increase in rare-earth doping decreases the conductivity. Since the ionic radii of rare earths are larger than that of $Zr^{4+}$, the free volume for oxide ion migration decreases with the increase of the rare-earth content, which explains the effect on conductivity.

The oxide ion conductivity linearly increases with reducing ionic radius of the dopant rare earth in the sequence Nd < Gd < Dy < Ho = Y < Er < Yb < Lu < Sc (Figure 27) as expected. Among the rare-earth-doped stabilized zirconias, the highest ion conductivity was obtained for the solid solution of $ZrO_2-Sc_2O_3$.

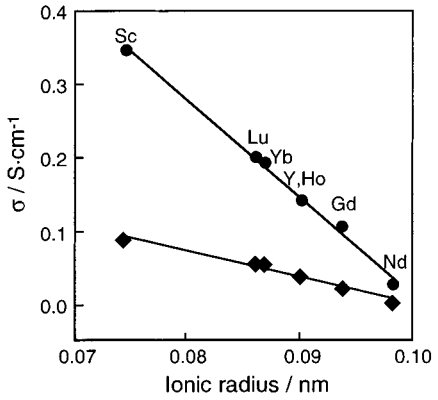


**Figure 27.** Relationship between the $O^{2-}$ ion conductivity and the doped rare-earth radius for stabilized zirconias at 800 (♦) and 1000 °C (●). (Reprinted with permission from ref 85. Copyright 1999 Springer-Verlag.)

Despite the observation that the oxide ion conductivity is the highest for $ZrO_2-Sc_2O_3$ among rare-earth-doped $ZrO_2$ solid solution series, the critical disadvantage is the low stability of the solid solution. An effective way to stabilize the solid solution is to add $Y_2O_3$, $Yb_2O_3$, or $Lu_2O_3$ to the $ZrO_2-Sc_2O_3$ solid solution which does not affect the oxide ion conductivity. The $ZrO_2$ solid solution mixed with another rare-earth oxide is much more stable than $ZrO_2$ with individual rare-earth oxide.[84]

The ternary system $ZrO_2-Sc_2O_3-Y_2O_3$ shows a higher conductivity than that of YSZ, and the degradation rate is much slower than that of scandia-stabilized zirconia (SSZ). The typical content of $YO_{1.5}$ and $ScO_{1.5}$ is 3−7mol % and up to 6 mol %, respectively.

Stabilized zirconia with ceria or praseodymia shows mixed conducting properties. In general, the electron transference number of these oxides is less than 0.1. Oxygen permeability and oxygen exchange properties of stabilized zirconia are also described in the literature.[85]

The addition of $Al_2O_3$ into $ZrO_2-Sc_2O_3-Y_2O_3$ where two different rare-earth species are introduced is also effective in making a composite, and it shows much better conductivity behavior in comparison to alumina-free materials.[86]

### 2. Bismuth Oxides

In $Bi_2O_3$, there are four polymorphs ($\alpha$, $\beta$, $\gamma$, $\delta$). The phase transformation from $\alpha$-phase to $\delta$-phase occurs at approximately 730 °C (Figure 28). The $\delta$-$Bi_2O_3$ phase is stable until it melts at about 825 °C. When $Bi_2O_3$ is cooled from the high-temperature $\delta$-$Bi_2O_3$ phase, a large hysteresis was observed and two intermediate metastable phases, tetragonal $\beta$-$Bi_2O_3$ and cubic $\gamma$-$Bi_2O_3$, are recognized. On cooling, the $\beta$-$Bi_2O_3$ phase appears at around 650 °C and the $\gamma$-$Bi_2O_3$ phase appears at 640 °C. The $\gamma$-$Bi_2O_3$ phase is stable down to room temperature, if the sample is cooled very slowly. In contrast, it is not possible to maintain the $\beta$-$Bi_2O_3$ phase and it transforms to $\alpha$-$Bi_2O_3$. The $\beta$-$Bi_2O_3$, $\gamma$-$Bi_2O_3$, and $\delta$-$Bi_2O_3$ phases all show mainly ionic conduction with the oxide anion as the charge carrier. The $\alpha$-$Bi_2O_3$ phase shows a variation in conductivity with oxygen pressure, and the main charge carrier is found to be a hole.

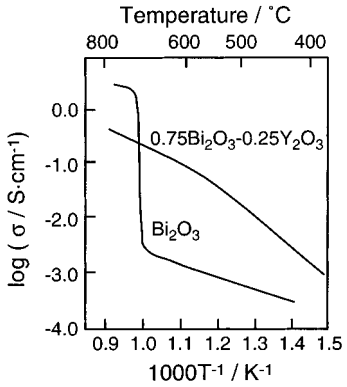


**Figure 28.** Temperature dependencies of the conductivity of $Bi_2O_3$ and $0.75Bi_2O_3-0.25Y_2O_3$.

The reasons of the high oxide anion conductivity in $\delta$-$Bi_2O_3$ are understood as follows: one-fourth of the oxygen sites are vacant in the $\delta$-$Bi_2O_3$ high-temperature phase which has the fluorite structure; $Bi^{3+}$ possesses $6s^2$ lone pair electrons and its high polarizability of the cation network allows oxide anions to migrate; $Bi^{3+}$ makes highly disordered surroundings.

The $Bi_2O_3-M_2O_3$ solid solutions showing high ionic conducting characteristics are categorized as cubic $\delta$-$Bi_2O_3$ or rhombohedral structure. Whether the cubic $\delta$-$Bi_2O_3$ or rhombohedral structure is formed is dependent on the dopant species and its concentration. The $Bi_2O_3-Gd_2O_3$ system belongs to both cubic and rhombohedral phases, and both are excellent oxide anion conductors.

The rhombohedral phase is formed in the case for larger $M^{3+}$ ions, while the cubic phases are, in general, formed for smaller cations. Among the $Bi_2O_3-R_2O_3$ (R = Y and/or rare earths) system, the $Bi_2O_3-Y_2O_3$ system has been investigated in the most detail. The $\delta$-$Bi_2O_3$ phase containing 25 mol % $Y_2O_3$ in $Bi_2O_3$ is stable at temperatures lower than 400 °C. The composition $0.75Bi_2O_3-0.25Y_2O_3$ is the lowest $R_2O_3$ composition where no phase transition occurs and composition maintains the highest conductivity over a wide region of temperature as shown in Figure 28.

The stability region of the high-temperature $\delta$-$Bi_2O_3$ phase is between 25 and 43 mol % $Y_2O_3$. When the content is less than 25 mol %, a significant hysteresis was observed between the heating and cooling process and the temperature difference is between 50 and 100 °C.

The ion conductivity of the $(Bi_2O_3)_{1-x}(R_2O_3)_x$ solid solution system for the minimum value of $x$ to stabilize the cubic phase vs ionic radius of $R^{3+}$ is plotted in Figure 29. The smallest $x_{min}$ value is obtained for $Er_2O_3$–stabilized $Bi_2O_3$ with the ionic transference number of unity, and it is clear that the $Bi_2O_3-Er_2O_3$ solid solution shows the highest ion conductivity. The value of $x_{min}$ increases with the ionic size. That is, a high $x_{min}$ value results in a low ionic conductivity.[87]

From an application point of view, stabilized $Bi_2O_3$ is not an appropriate candidate for SOFC electrolyte,

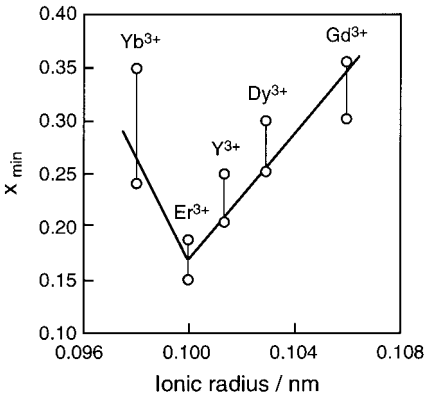


**Figure 29.** Ion conductivity of the $Bi_2O_3-M_2O_3$ solid solution system for the minimum value of $x$ to stabilize the cubic phase vs ionic radius of $M^{3+}$. (Reprinted with permission from ref 87. Copyright 1999 Elsevier Science Ltd.)

due to the reduction in a low $pO_2$ environment. The thermodynamic stability of $Bi_2O_3$ solid electrolyte along with phase stability at low temperatures are also required.[88]

### 3. Thorium Oxides

Thorium oxide ($ThO_2$) possesses a fluorite structure, and the addition of rare-earth oxides introduces anion vacancies. While $Sc_2O_3$ can only make a solid solution with $ThO_2$ at low $Sc_2O_3$ contents, other lighter lanthanide oxides in which rare-earth ionic radii are appreciably larger than that of Sc are very soluble in $ThO_2$. The cations of the rare-earth oxides holding a C-type structure do not show a complete miscibility with $ThO_2$ due to their small ionic size. In addition, $ThO_2$ shows a greater stability compared with $ZrO_2$ in a highly reducing atmosphere where n-type conduction becomes significant for $ZrO_2$-based electrolytes. The unusually high stability of $ThO_2$-based solid electrolytes is an outstanding advantage compared to $ZrO_2$-based electrolyte, especially for application in a low oxygen pressure region. $ThO_2$-based solid electrolytes are chemically very inert, and $ThO_2$ shows an excellent corrosion resistance in molten alkaline metals such as molten sodium. Impurities in $ThO_2$ usually result in electronic conduction because of the introduction of energy levels near the conduction band. Therefore, the purity of the starting materials is essential for the case of $ThO_2$ in considering it in the solid electrolyte field.

### 4. Hafnium Oxides

Another candidate element which is located in the same IV A group in the periodic table but having a higher atomic number than Zr is Hf. Figure 30 shows the relationship between the ion transference number ($t_{ion}$) and the oxygen pressure for $HfO_2$-based fluorite solid electrolyte at 1600 °C. The data of CaO-doped zirconia is also plotted. From the figure it becomes clear that the $HfO_2$-based electrolytes are preferable for use at high temperatures and in the low oxygen pressure region. Electronic conductivity is negligible, indicating a suitability for fully killed steel melts condition (compared with the $ZrO_2$-based electrolytes which show n-type electronic conduction and are not applicable). Another way of obtaining a low oxygen

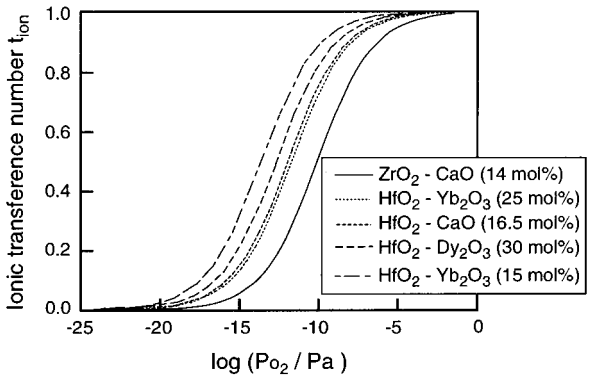


**Figure 30.** Relation between the ion transference number ($t_{ion}$) and the oxygen pressure for $HfO_2$-based solid electrolytes at 1600 °C. (Reprinted with permission from ref 89. Copyright 1996 American Ceramic Society.)

pressure application is to use the ternary electrolyte of $HfO_2-ZrO_2-Y_2O_3$ and $HfO_2-ThO_2-Y_2O_3$.[89]

### 5. Apatites

The calcium oxyhydroxyapatites, $Ca_{10-x}R_x(PO_4)_6(OH)_{2-x}O_x$ ($R = Y^{3+}$ or $La^{3+}$), show ion conducting behavior. Among these, the highest conductivity is obtained for $Ca_{9.3}Y_{0.7}(PO_4)_6(OH)_{1.3}O_{0.7}$. For $x$ appreciably larger than 1, the dominant charge carrier is $O^{2-}$, while in the range of $0 < x < 1$, mobile ions are $OH^-$ and $O^{2-}$. However, there still remains a possibility of proton conduction through $OH^-$.[90]

Since rare-earth-based apatites show a considerable oxide anion conductivity, various types of stoichiometric compounds have been investigated in addition to the stoichiometric compound $(R_{0.8}A_{0.2})_{10}(MO_4)_6O_2$. One type is the cation-deficient compound $R_{9.33}(MO_4)_6O_2$; the other is the oxygen excess compound of $R_{10}(MO_4)_6O_3$ and $(R_{10-x}A_x)(MO_4)_6O_{3-x/2}$ (R = La, Nd, Sm, Gd, Dy; A = Ca, Sr, Ba; and M = Si, Ge).

The $R_{10}(SiO_4)_6O_3$ (R = La, Nd, Sm, Gd, Dy, Y, Ho, Er, and Yb) series has been demonstrated to be good oxide anion conductors. The structure is composed of interconnecting $LaO_6$ octahedra and $SiO_4$ tetrahedra comprising a three-dimensional network structure.

The electrostatic interaction between the oxygen and $Ln^{3+}$ reduces with increasing $Ln^{3+}$ ion radius. Among the series, the compound with La shows the highest conductivity. Figure 31 presents the relation between the ionic radius and the electrical properties of $R_{10}(SiO_4)_6O_3$. With increasing ionic radius of $R^{3+}$ in $R_{10}(SiO_4)_6O_3$, the activation energy decreases and the conductivity increases. The maximum conductivity of $1.4 \times 10^{-3}$ S·cm$^{-1}$ was obtained for $La_{10}(SiO_4)_6O_3$ at 700 °C. As can be seen, the conductivity of $R_{10}(SiO_4)_6O_3$ with monoclinic structure (R = Y, Ho, Er, Yb) is appreciably lower than that of the samples with hexagonal structure (R = La, Nd, Sm, Gd, Dy). The oxide ion transference number of $R_{10}(SiO_4)_6O_3$ with R = Nd and Sm was investigated, and it was found to be almost unity at >600 and >700 °C, respectively. Although $La_{10}(SiO_4)_6O_3$ shows the highest conductivity, microcracks appear in the bulk, and this makes it impossible to conduct the electromotive

**Table 1. Comparison of the Experimental Methods which Have Been Applied (×) or Not (−) To Characterize the Compounds for which a Multivalent Cationic Conduction Is Assumed[a]**

| ionic conducting compound | impedance spectroscopy | polarization measurements | conductivity or polarization in different atmosphere | EMF measurements | DC electrolysis + detailed analysis | Tubandt or related electrolysis |
|---|---|---|---|---|---|---|
| $M^{3+}$−$\beta''$-alumina (IE) | × | − | − | − | − | − |
| $M^{3+}$−$\beta$-alumina (DS) | × | × | − | × | − | − |
| $\beta$-alumina-related phases | × | − | − | × | − | − |
| $\beta$-$LaNb_3O_9$ | × | × | × | × | − | − |
| $Sc_2(WO_4)_3$-type phases | × | × | × | × | × | × |

[a] $\beta$-Alumina compounds which are prepared by ion exchange or by direct synthesis are denoted by IE and DS, respectively.

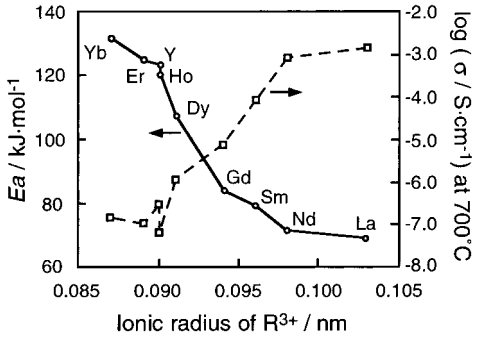


**Figure 31.** Relationship between the ionic radius and the electrical properties of $R_{10}(SiO_4)_6O_3$. (Reprinted with permission from ref 92. Copyright 1995 Royal Society of Chemistry.)

force (EMF) measurement due to the gas permeation.[91, 92]

In $La_{9.33}Si_6O_{26}$, a considerable number (ca. 14%) of oxygen atoms are displaced from the ideal position, which creates Frenkel-like defects. In addition, in the channel sites, disorder is also observed.[93] Therefore, these compounds possess a comparable conductivity to or higher than that of yttria-stabilized zirconia at 600 °C and show a high oxide ion transference number of higher than 0.9 in a wide oxygen partial pressure region of $10^5$−$10^{-16}$ Pa with low activation energy of 0.6−0.8 eV. They are potentially useful, especially for a low or intermediate temperature range of operation.[94] However, a significant disadvantage is the instability of the $La_{9.33}Si_6O_{26}$ solids in comparison to the commonly known stabilized zirconia.

## IV. Trivalent Cation Conductors

Up to now, the conducting ion species in solid electrolytes introduced are mainly limited to mono- and divalent ions because the ionic conductivity strongly depends on their valency. For trivalent cations, the electrostatic interaction between the conducting trivalent cation and surrounding anions has been believed to be too strong to realize a trivalent ion migration in a solid lattice. Therefore, trivalent cations such as rare-earth ions in solid electrolytes are commonly used for adjustment of the defect concentration and the lattice size. For realizing the trivalent cation conduction in a solid lattice, it is necessary to reduce such a strong interaction between the mobile trivalent cation and the lattice forming anions. Some papers have claimed that $Ln^{3+}$−$\beta$/$\beta''$-alumina,[35−37,95−107] $\beta$-alumina-related materials,[108−112] and $Ln^{3+}$−$\beta$-$LaNb_3O_9$,[20,113] are trivalent ion conductors. However, these reports have neither directly nor quantitatively demonstrated any trivalent ion migration in solids as listed in Table 1. The methods utilized for $Ln^{3+}$−$\beta''$-alumina, $\beta$-$LaNb_3O_9$, and $LaAl_{11}O_{18}$ are indirect and not quantitative. Among them, especially, $Ln^{3+}$−$\beta''$-alumina solid electrolytes were prepared by ionically exchanging the $Na^+$ site in $Na^+$−$\beta''$-alumina for $Ln^{3+}$. Therefore, a small amount of $Na^+$ ion still remains in these solid electrolytes and might contribute to ion conduction. Recently, $M_2(M'O_4)_3$ (M = Al, In, Sc, Y, Er−Lu; M′ = W, Mo) solid electrolytes with orthorhombic $Sc_2(WO_4)_3$-type structure were shown to have trivalent $M^{3+}$ cation conducting characteristics.[114−134] The $Sc_2(WO_4)_3$-type structure is a quasi-layered structure and has a large pathway where $M^{3+}$ ion can migrate smoothly, and the hexavalent tungsten ion bonds to four surrounding oxide anions to form a rigid $WO_4^{2-}$ tetrahedral unit. This results in a considerable reduction of the electrostatic interaction between $M^{3+}$ and $O^{2-}$ and the realization of the $M^{3+}$ ion conduction.

In 1999, a new trivalent rare-earth conducting solid electrolyte with NASICON-type structure[135−139] was reported as an advanced trivalent cationic conductor, which is one of the appropriate candidates for practical applications.

### A. $Ln^{3+}$−$\beta$-aluminas and $Ln^{3+}$−$\beta''$-aluminas

As for trivalent cations, a trivalent ion exchange into the conduction planes of $Na^+$−$\beta''$-alumina crystals is also possible and has been performed for various kinds of cations including Bi,[37,95,96] Cr,[95] La,[97] Pr,[37,96,98−100] Nd,[37,95,96] Sm,[37,95,96] Eu,[37,95,96] Gd,[37,95,96] Tb,[37,95,96] Dy,[37,96] Ho,[101] Er,[95,96] and Yb.[37,95] $Gd^{3+}$−$\beta''$-$Al_2O_3$ was prepared by the usual exchange reaction method (the degree of ion exchange is listed in Table 2) and claimed to be a solid electrolyte with trivalent

**Table 2. Degree of Ion Exchange for $M^{3+}$−$\beta''$-Alumina Crystals**

| trivalent ion species | degree of exchange | ref | trivalent ion species | degree of exchange | ref |
|---|---|---|---|---|---|
| $La^{3+}$ | 98 | 97 | $Tb^{3+}$ | 90 | 37 |
| $Pr^{3+}$ | 43 | 37 | $Ho^{3+}$ | 98 | 101 |
| $Nd^{3+}$ | 95 | 103 | $Er^{3+}$ | 96 | 95 |
| $Sm^{3+}$ | 90 | 37 | $Yb^{3+}$ | 90 | 37 |
| $Eu^{3+}$ | 95 | 37 | $Bi^{3+}$ | 70 | 37 |
| $Gd^{3+}$ | 100 | 37 | $Cr^{3+}$ | 75 | 95 |

cationic conduction. Although $Gd^{3+}$−$\beta''$-alumina is an insulator at room temperature ($\sigma_{rt} < 10^{-11}$ S·cm$^{-1}$) because $Gd^{3+}$ ions within the conduction plane are locked in bonds to oxygen between the spinel blocks,

the conductivity at elevated temperatures increases and is assumed to result from a $Gd^{3+}$ ion transport, generating a conductivity of $10^{-3}$ S·cm$^{-1}$ at 600−700 °C.[96] For other lanthanide ion (Ln = La, Pr, or Nd) exchanged $Ln^{3+}$−$\beta''$-alumina crystals, conductivity values of $10^{-4}$−$10^{-6}$ S·cm$^{-1}$ have been reported for temperatures around 400−500 °C. However, the identity of the charge carrier in these solids was not conclusively identified. Since these $Ln^{3+}$−$\beta''$-aluminas are prepared by an ion exchange method, a small amount of $Na^+$ ion may still remain despite the authors' claim that the ion exchange ratio is ca. 100% (for example, the composition of $Gd^{3+}$−$\beta''$-alumina crystal, which was almost completely ion-exchanged, has been identified by labeling the original $Na^+$ ion content of the starting crystal with $^{22}Na$ so that the remaining sodium ion content can be identified). For other highly ion-exchanged $\beta''$-alumina with $La^{3+}$ (98%), $Ho^{3+}$ (98%), and $Er^{3+}$ (96%) (see Table 2), at least 2% or 4% $Na^+$ still remains, and the remaining $Na^+$ ions contribute predominantly to the ion conduction in the $\beta''$-alumina solids. Furthermore, the presence of divalent $Mg^{2+}$ cations in the spinel blocks must be speculated to conduct in the solid as well. Therefore, the conducting candidate species are $Ln^{3+}$, $Mg^{2+}$, remaining $Na^+$ cations, protons, oxide anions, and electronic charge carrier. Unfortunately, the ion-exchanged $Ln^{3+}$−$\beta''$-aluminas have not been directly identified to be $Ln^{3+}$ ion conductors by experimental procedures. Only electrical conductivity and XRD measurements are performed, and they conclude them to be the trivalent cationic conductors. The activation energy at lower temperature for all samples derived from the Arrhenius plot was very low in comparison with those in the higher temperature region. As an example, the temperature dependencies of the conductivity for ion-exchanged $Na^+/Ho^{3+}$−$\beta''$-alumina[101] are depicted in Figure 32. The activation

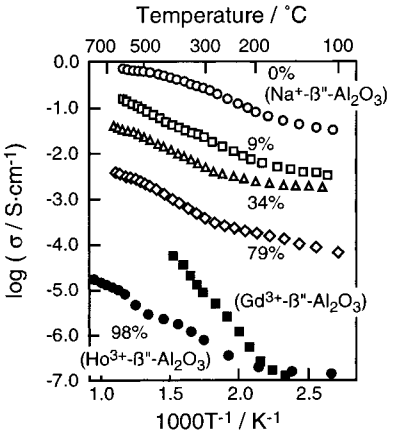


**Figure 32.** Temperature dependencies of the conductivity for ion-exchanged $Na^+/Ho^{3+}$−$\beta''$-alumina with the data of $Gd^{3+}$−$\beta''$-alumina. (Reprinted with permission from ref 101. Copyright 1995 Elsevier Science B. V.)

energies for 98% ion-exchanged $Na^+/Ho^{3+}$−$\beta''$-alumina are 0.058 eV at 150 °C and 0.456 eV at 500 °C. For the purpose of investigating this unique behavior in ion-exchanged $Ln^{3+}$−$\beta''$-alumina, the $Ln^{3+}$ cation occupation in the conduction plane of $\beta''$-alumina structure was extensively studied by using X-ray diffraction for $Pr^{3+}$−$\beta''$-alumina at temperatures between 25 and 500 °C.[101] From these measurements it was found that the only 10% $Pr^{3+}$ occupied the BR sites at room temperature and the BR position occupancy was increased up to 250 °C where both BR and mO sites are occupied to a nearly equal extent. At even higher temperatures, a redistribution of $Pr^{3+}$ back into mO sites was again observed. Therefore, it seems to be difficult for $Pr^{3+}$ to migrate at low temperature because the $Pr^{3+}$ ions are trapped within the BR site and unable to exhibit a long-range migration due to considerably high potential barriers of the nonequivalent BR and mO sites. The result is that the residual $Na^+$ ions may migrate. However, at high temperatures, the $Pr^{3+}$ ion is able to obtain an enough energy to overcome the barriers and to migrate out of BR into the next mO sites.

Recently dc electrolysis was performed for $Nd^{3+}$−$\beta''$-alumina (degree of exchange was ca. 98%) at both 250 and 650 °C in order to directly clarify the conducting species in ionically exchanged $Ln^{3+}$−$\beta''$-alumina.[103] A schematic illustration of the setup of dc electrolysis for $Nd^{3+}$−$\beta''$-alumina is shown in Figure 33. The line electron probe micro analysis

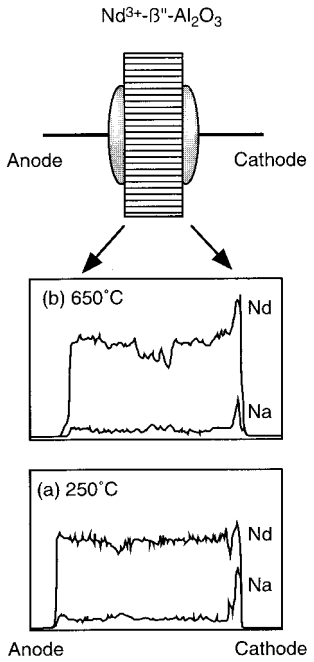


**Figure 33.** Schematic illustration of the setup of dc electrolysis for $Nd^{3+}$−$\beta''$-alumina and the EPMA line analysis results for $Nd^{3+}$−$\beta''$-alumina which were electrolyzed at both 250 °C (a) and 650 °C (b). (Reprinted with permission from ref 103. Copyright 2000 WILEY−VCH Verlag GmbH.)

(EPMA) was performed for the $Nd^{3+}$−$\beta''$-aluminas, which were electrolyzed at both 250 (Figure 33a) and 650 °C (Figure 33b). The significant segregation of Nd atoms was not observed at the cathodic surface for the sample electrolyzed at 250 °C, while Na atoms significantly segregated. On the other hand, for the sample heated to 650 °C, a strong Nd peak was also recognized together with a Na peak. These results clearly indicate that the migrating species in $Nd^{3+}$−$\beta''$-alumina is $Na^+$ and $Na^+/Nd^{3+}$ at lower and higher temperatures, respectively, and that the ion-exchanged $Nd^{3+}$−$\beta''$-alumina is not a pure trivalent

$Nd^{3+}$ cationic conductor but $Na^+$ and $Nd^{3+}$ mixed ion conductor at elevated temperatures. In other ion-exchanged $Ln^{3+}-\beta''$-aluminas there is also doubt as to whether only the $Ln^{3+}$ cation migrates or not by the same reason as for $Nd^{3+}-\beta''$-alumina.

The ion exchange into $Na^+-\beta''$-alumina polycrystal is much more difficult than for single crystalline material, in particular for the case of trivalent cations. Therefore, trivalent ion exchange reactions for polycrystalline $Na^+-\beta''$-alumina have been rarely reported, e.g., only for the $Na^+/Nd^{3+}-\beta''$-alumina[104] and the $Na^+/Ce^{3+}-\beta''$-alumina[36] systems. However, electrical conductivity measurements were not conducted on these samples. Furthermore, the grains of the latter compound exhibit microcracks due to expansion in the crystal structure which occur when the large lanthanide ions substitute for $Na^+$ for $Nd^{3+}$ into the conduction planes.

As for the $\beta$-alumina, the $Ln^{3+}-\beta$-aluminas (Ln = Pr, Nd, Ho) were synthesized by an ion exchange method.[105−107] However, the ion exchange of $Ln^{3+}$ for $Na^+$ in $\beta$-alumina is difficult since the structural characteristics as well as mechanisms of charge compensation differ from $\beta$-alumina to $\beta''$-alumina, and the degree of exchange ratio was, therefore, only 95% at maximum. The low ion exchange seems to be due to the excess amount of $Na^+$ ion compensated by interstitial $O^{2-}$ ions in the conduction planes. The ionic conduction properties of $Ln^{3+}-\beta$-aluminas were not investigated at all.

## B. $\beta$-Alumina-Related Materials

It is also possible to replace $Al_2O_3$ within the spinel framework by other oxides, such as $Ga_2O_3$, forming the corresponding isomorphous $\beta$- or $\beta''$-gallates,[140,141] respectively. The $\beta/\beta''$-gallates often exhibit faster ionic conductivity than the corresponding $\beta/\beta''$-aluminas. The faster ion exchange occurs due to the larger ionic radius of $Ga^{3+}$ (0.076 nm; CN = 6[26]) than that of $Al^{3+}$ (0.0675 nm; CN = 6[26]), whose ion appears in the spinel blocks. The large $Ga^{3+}$ cation in the spinel block causes the enlargement of the space between the two adjacent spinel blocks. As a consequence, the steric hindrance for the conducting cations is reduced, resulting in faster ion exchange. However, since the gallates do not have the same thermal stability as the $\beta$-alumina in addition to its high cost, its application is limited.

Magnetoplumbite-type ($A^{2+}B^{3+}{}_{12}O_{19}$) compound is another related material. The structure is shown in Figure 34. In the magnetoplumbite structure, a mirror plane sandwiched between two spinel blocks is similar to $\beta/\beta''$-$Al_2O_3$. These magnetoplumbite-type materials are easily obtained by a conventional solid-state reaction methods. However, the mirror plane has no oxygen vacancies and ions are more densely packed compared to $\beta/\beta''$-$Al_2O_3$. Owing to these factors, the magnetoplumbite-type compounds exhibit a considerably lower conductivity and a higher activation energy than $\beta/\beta''$-$Al_2O_3$. For the magnetoplumbite-type solid electrolytes with lanthanoid atoms, $LnAl_{11}O_{18}$ (Ln = La, Ce, Pr, Nd, Sm, Eu) and $LnAl_{12}O_{18}N$ (Ln = La, Ce, Pr, Nd, Sm, Eu, Gd) were

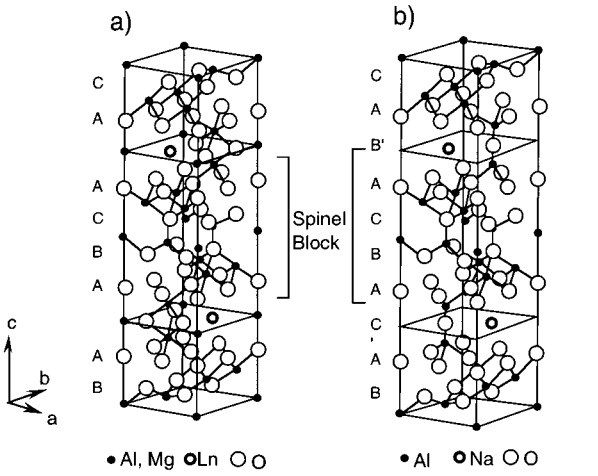


**Figure 34.** Comparison of the hexagonal crystal structures of the magnetoplumbite phase $LaMgAl_{11}O_{19}$ (a) and $Na^+-\beta$-$Al_2O_3$ (b). (Reprinted with permission from ref 10. Copyright 1998 American Chemical Society.)

reported.[108−112] From impedance spectroscopic and EMF measurement results, trivalent lanthanide cation conduction was assumed. However, similar to the case for $Ln^{3+}-\beta''$-alumina, a direct demonstration of trivalent cation, which denies the possible migration of oxide anion and proton, etc., has not been carried out yet.

## C. Perovskite-Type Structures

Trivalent cationic conduction in perovskite structure was reported for $\beta$-$LaNb_3O_9$.[113] The compound is A-site deficient, which is one of key points of high valency cation conduction. $La^{3+}$ ions are surrounded by 12 oxygen atoms adopting an ordered distribution. One of the A-sites located in the plane parallel to the *ab* plane is entirely empty, and one is statistically occupied by 2/3 of the lanthanum ions as already illustrated in Figure 5. The vacant A-positions are energetically equivalent and double the number of total $La^{3+}$ ions in the lattice, therefore providing an interconnected 3D-channel for the assumed ionic motion. The $\beta$-$LaNb_3O_9$ is a mixed ionic−electronic conductor, and the electronic conduction appears at temperatures higher than 577 °C, while it is reported that the $La^{3+}$ predominantly conducts below 577 °C. dc electrolysis of $\beta$-$LaNb_3O_9$ was performed to demonstrate $La^{3+}$ migration in the solid. After electrolysis, the color change of both the cathodic and anodic surfaces and a high concentration of La atom at only the cathodic surface was observed. However, the electrolysis was done at ca. 727 °C, which is higher than the ambit temperature of ionic and electronic conduction. Therefore, it seems that the sample decomposed. Furthermore, since the material, which is expected to segregate at the cathodic surface by the cation migration, was not identified at all, it is still questionable whether $\beta$-$LaNb_3O_9$ can be called a "pure" trivalent cationic conductor or not.

In 2000, a new trivalent $Y^{3+}$ ion conducting solid electrolyte with A-site-deficient perovskite structure, $Y_x(Ta_{3x}W_{1-3x})O_3$ ($0 \leq x \leq 0.33$),[142] was reported by Sato et al. By substituting the pentavalent $Ta^{5+}$ site for

hexavalent $W^{6+}$ in $Y_{1/3}TaO_3$[21,143−145] which holds the perovskite structure, A-site cations, such as $Y^{3+}$, are completely lacking on alternate layers and $Y^{3+}$ vacancies are introduced. In the $Y_x(Ta_{3x}W_{1-3x})O_3$ series, $Y_{0.06}(Ta_{0.18}W_{0.82})O_3$ ($x = 0.06$) shows the highest conductivity (ca. $2.58 \times 10^{-5}$ S·cm$^{-1}$ at 362 °C), which is about 400 and 800 times higher than that of $La_{1/3}NbO_3$ and $La_{1/3}TaO_3$, respectively. The polarization behavior for $Y_x(Ta_{3x}W_{1-3x})O_3$ was investigated, and a clear polarization was obtained. As a result, $Y_x(Ta_{3x}W_{1-3x})O_3$ was claimed to be a $Y^{3+}$ ion conductor because a good polarization phenomenon in oxygen atmosphere indicates that no $O^{2-}$ anion conduction appears and the high-valent $Ta^{5+}$ and $W^{6+}$ ions are considered to be difficult to migrate in the solid. However, the polarization measurements in $O_2$ atmosphere indicate only the impossibility of oxide anion conduction, and the experiments applied for $Y_x(Ta_{3x}W_{1-3x})O_3$ are still insufficient for the demonstration of trivalent cation migration in the solid.

## D. $Sc_2(WO_4)_3$-Type Solid Electrolytes

The tungstate with trivalent cation, $M_2(WO_4)_3$, has two crystal structures depending on the trivalent cation size as shown in Figure 35.[146] One is a $Sc_2(WO_4)_3$-type structure with orthorhombic symmetry, and the other is a monoclinic $Eu_2(WO_4)_3$-type structure. The $Sc_2(WO_4)_3$-type structure has a quasi-layered one and a large pathway where $M^{3+}$ ion can migrate smoothly as shown in Figure 36. In this structure, hexavalent tungsten ion ($W^{6+}$) bonds to four surrounding oxide anions to form a rigid $WO_4^{2-}$ tetrahedron unit, resulting in a considerable reduction of the electrostatic interaction between $M^{3+}$ and$O^{2-}$ and the realization of the $M^{3+}$ ion conduction. On the other hand, while $Eu_2(WO_4)_3$-type structure also contains $W^{6+}$, the trivalent cation in $Eu_2(WO_4)_3$-type structure is 8-coordinate ($M^{3+}$ in $Sc_2(WO_4)_3$-type structure is 6-coordinate). Therefore, $M^{3+}$ cannot migrate in a $Eu_2(WO_4)_3$-type lattice due to the stronger electrostatic interaction with eight oxide anions.

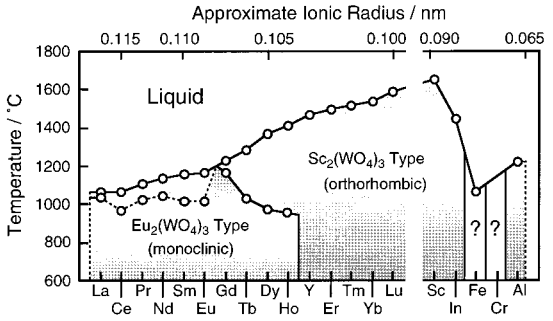


**Figure 35.** Structure type of tungstates with trivalent cation, $M_2(WO_4)_3$. (Reprinted with permission from ref 146. Copyright 1971 Academic Press.)

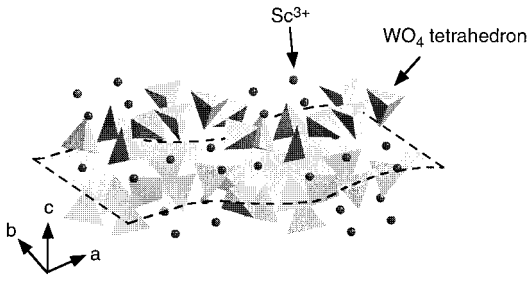


**Figure 36.** Quasi-layered $Sc_2(WO_4)_3$-type structure. The shade plane surrounded by dashed line presents one of the ion conducting path planes (*ab* plane).

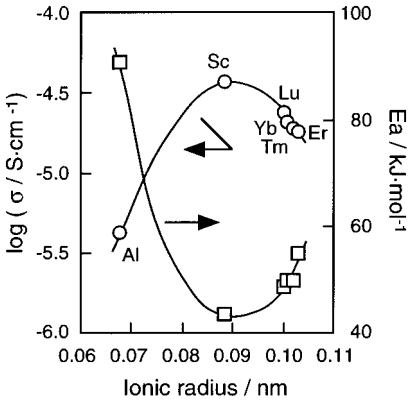


**Figure 37.** Electrical conductivities at 600 °C and activation energies for $M_2(WO_4)_3$ with $Sc_2(WO_4)_3$-type structure. (Reprinted with permission from ref 119. Copyright 1998 American Chemical Society.)

Figure 37 shows the electrical conductivities at 600 °C and activation energies for $M_2(WO_4)_3$ with $Sc_2(WO_4)_3$-type structure. The conductivity of $M_2(WO_4)_3$ changes with the variation of ionic radius, and $Sc_2(WO_4)_3$ shows the highest conductivity among the $M_2(WO_4)_3$ series. In solid electrolytes with trivalent $M^{3+}$ ion larger than $Sc^{3+}$, the conductivity decreases because the conducting $M^{3+}$ cation size becomes disproportionately large compared with the lattice size. On the other hand, for the ion species of $Al^{3+}$ which has a much smaller ionic radius (0.0675 nm; CN = 6[26]) in comparison with the $Sc^{3+}$ (0.0885 nm; CN = 6[26]), the ion conductivity decreased considerably due to the larger contraction of the volume of the migrating trivalent ion from $Sc^{3+}$ to $Al^{3+}$ compared with that of the crystal lattice from $Sc_2(WO_4)_3$ to $Al_2(WO_4)_3$.

Trivalent cation conduction in $Sc_2(WO_4)_3$-type solid electrolyte was directly demonstrated by the measurements of oxygen pressure dependencies of the electrical conductivity, polarization measurement, and dc electrolysis. All samples which hold the $Sc_2(WO_4)_3$-type structure show the constant conductivity in a wide oxygen pressure range, which indicates that no electronic conduction appears in the sample. The dc conductivity of the samples was measured in a different oxygen partial pressure atmosphere, and the dc to ac conductivity ratio was drastically decreased with passing time. This phenomenon clearly shows that the probability of oxide anion conduction in solid was eliminated because if $O^{2-}$ anion is a migrating species, the dc conductivity should be equal to the ac conductivity and the above-mentioned ratio should be unity. This should be independent of the time exposure in $O_2$ atmosphere where the migrating

species is constantly provided. The ionic transference number, $t_{ion}$, calculated from the value at 10 min after electrolysis, was 0.99. The EMF measurement of the $O_2$ concentration cell using $Sc_2(WO_4)_3$ was also conducted in various temperatures with the aim of excluding the electronic conduction. The measured EMF is in excellent agreement with the theoretical value calculated from Nernst equation, and $t_{ion}$ was estimated to be unity.

For the purpose of identifying the conducting cationic species in $Sc_2(WO_4)_3$, dc electrolysis was performed by applying a dc voltage of 10 V, which is higher than the decomposition voltage of $Sc_2(WO_4)_3$ (ca. 1.2 V) with Pt as an ion blocking electrode. Figure 38 shows the scanning electron microscope (SEM)

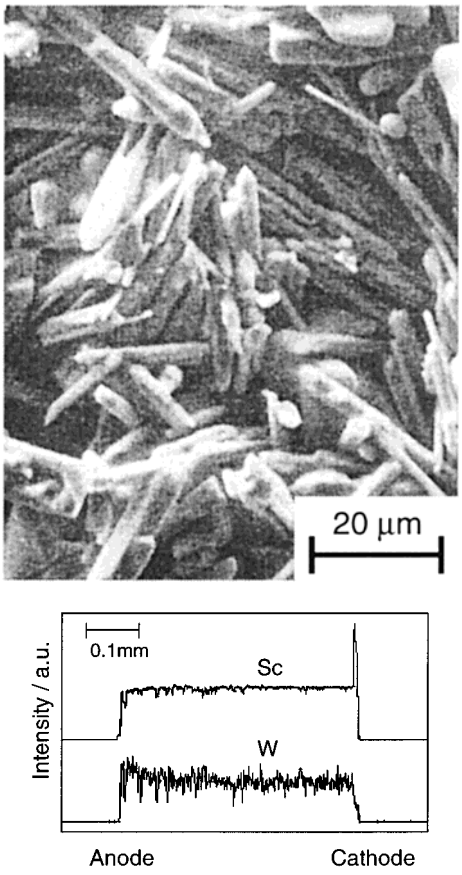


**Figure 38.** SEM image at the cathodic surface of the electrolyzed pellet and the result of EPMA line analysis for the $Sc_2(WO_4)_3$ solid. (Reprinted with permission from ref 119. Copyright 1998 American Chemical Society.)

image at the cathodic surface of the electrolyzed pellet and the result of an EPMA line analysis for $Sc_2(WO_4)_3$ solid electrolyte. After dc electrolysis, the needle on the material included an amount of Sc that was 9 times higher than that in the mother bulk $Sc_2(WO_4)_3$ which identified to be $Sc_6WO_{12}$ at the cathodic surface. On the other hand, the color at the anodic surface of the electrolyzed sample changed to yellow and $WO_3$ was detected. Furthermore, a strong Sc peak was detected at only the cathodic surface. These results strongly indicate that the following reaction occurred during dc electrolysis and the macroscopic migration of $Sc^{3+}$ in $Sc_2(WO_4)_3$.

$$\text{(anodic surface) } Sc_2(WO_4)_3 \rightarrow 2Sc^{3+} + 3WO_3 + {}^3/_2O_2 + 6e^- \quad (5)$$

$$\text{(cathodic surface) } 2Sc^{3+} + 6e^- \rightarrow 2Sc \quad (6)$$

$$2Sc + {}^3/_2O_2 \rightarrow Sc_2O_3 \quad (7)$$

$${}^8/_3Sc_2O_3 + {}^1/_3Sc_2(WO_4)_3 \rightarrow Sc_6WO_{12} \quad (8)$$

To demonstrate macroscopic trivalent cation conduction in tungstates, dc electrolysis was carried out by using two tungstates of $Al_2(WO_4)_3$ and $Sc_2(WO_4)_3$ (the setup is presented in Figure 39). After the

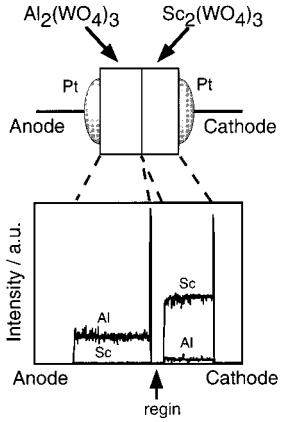


**Figure 39.** Setup of dc electrolysis and EPMA line analysis for the $Sc_2(WO_4)_3$ solid electrolyte with $Al_2(WO_4)_3$. (Reprinted with permission from ref 116. Copyright 1998 Electrochemical Society Inc.)

electrolysis, Al clearly existed inside the $Sc_2(WO_4)_3$ bulk where no Al atom appears before electrolysis, as shown in Figure 39. This phenomenon clearly indicates that $Al^{3+}$ ion migrated from $Al_2(WO_4)_3$ (anodic side) to $Sc_2(WO_4)_3$ (cathodic side).

The trivalent $Al^{3+}$ ion conducting properties in $Al_2(WO_4)_3$ single crystal with $Sc_2(WO_4)_3$-type structure were measured. A large-sized $Al_2(WO_4)_3$ single crystal (15 mm in diameter and up to 35 mm in length) with high transparency was successfully grown by modified Czochralski (CZ) method.[120] The $Al^{3+}$ ion conducting behavior should be different parallel to each of the these crystals since the $Sc_2(WO_4)_3$-type structure is orthorhombic. It was found that the ion conductivity along the *b*-axis was the highest conductivity among the three axes. The conductivity along the *b*-axis at low temperature (<500 °C) was higher than that of polycrystalline sample. The conductivity along the *c*-axis is about 2 orders of magnitude lower than that of the *b*-axis. Therefore, the $Sc_2(WO_4)_3$ series is expected to show the highest ion conductivity along the *b*-axis.

Various kinds of solid solution with $Sc_2(WO_4)_3$-type structure were also extensively investigated for the purpose of enhancing the trivalent ion conductivity of the tungstates. Figure 40 shows the electrical conductivities of $(1-x)Sc_2(WO_4)_3-xLn_2(WO_4)_3$ (Ln = Lu,[124] Gd[117]) at 600 °C. For the $Lu^{3+}$ system, the discontinuity of the conductivity is recognized between $x = 0.5$ and 0.6. From dc electrolysis of the samples with the composition $x = 0.4$ and 0.6, the

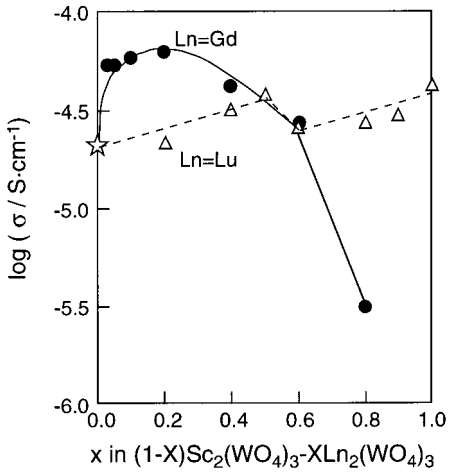


**Figure 40.** Electrical conductivities of $(1-x)Sc_2(WO_4)_3-xM_2(WO_4)_3$ (M = Lu, Gd) at 600 °C.

Sc/Lu ratio at the cathodic surface changed from 0.76 (before electrolysis) to 1.14 (after electrolysis) and from 0.48 to 0.40, respectively. These results clearly confirm that the predominant conducting species was $Sc^{3+}$ at the range of $x$ smaller than 0.5 and the charge carrier changes to $Lu^{3+}$ at the higher $x$ region. On the other hand, the conductivity of the Gd system drastically decreased at around $x = 0.7$. This decrease occurs because of the structural change from $Sc_2(WO_4)_3$- to $Eu_2(WO_4)_3$-type as suggested by Figure 35.

To enhance the conductivity of $Al_2(WO_4)_3$, the $Al_2(WO_4)_3-Sc_2(WO_4)_3-Lu_2(WO_4)_3$ solid solutions were prepared.[118] Figure 41 shows the electrical conductivity at 600 °C for the obtained solid solutions. Among the solutions investigated, the $0.1(Al_2(WO_4)_3)-0.9((Sc_{0.5}Lu_{0.5})_2(WO_4)_3)$ solid solution shows the highest electrical conductivity of $8.71 \times 10^{-5}$ S·cm$^{-1}$ (log $\sigma$ = -4.06), and the conductivity is approximately 25 times higher than that of pure $Al_2(WO_4)_3$ ($3.39 \times 10^{-5}$ S·cm$^{-1}$) (log $\sigma$ = -5.47). The conducting trivalent species in the $0.1(Al_2(WO_4)_3)-0.9((Sc_{0.5}Lu_{0.5})_2(WO_4)_3)$ solid solution was directly investigated by dc electrolysis and followed by SEM observation and EPMA. After electrolysis, the $Al_2O_3$ deposits were observed only at the cathodic surface. From the EPMA line analysis of the electrolyzed pellet, only a considerable $Al^{3+}$ segregation appeared on the cathodic surface while other cations were homogeneously distributed from the anodic to cathodic surfaces. These results mean that the $Al^{3+}$ ion migration is much easier than the ionic migrations of $Sc^{3+}$, $Lu^{3+}$, and also $W^{6+}$ in the $Sc_2(WO_4)_3$-type structure.

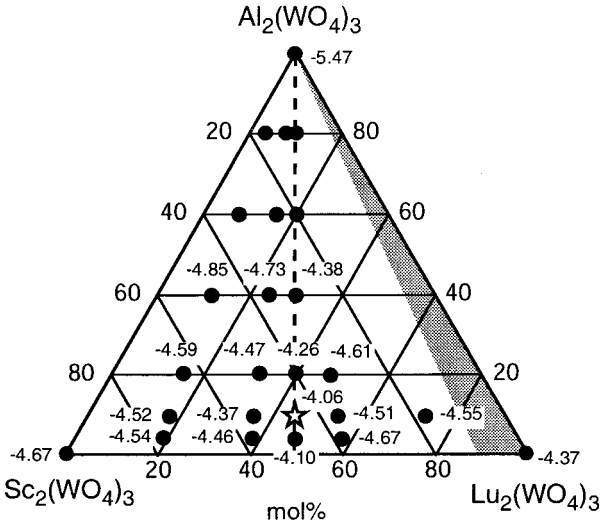


**Figure 41.** Electrical conductivity at 600 °C for the obtained $Al_2(WO_4)_3-Sc_2(WO_4)_3-Lu_2(WO_4)_3$ solid solutions. (Reprinted with permission from ref 118. Copyright 1998 American Chemical Society.)

Molybdates with $Sc_2(WO_4)_3$-type structure, $M_2(MoO_4)_3$, were also prepared. Their trivalent $M^{3+}$ conductivities were higher than those of tungstates as shown in Figure 42 due to the smaller ionic radius of $Mo^{6+}$ (0.055 nm; CN = 4[26]) and $W^{6+}$ (0.056 nm; CN = 4[26]), resulting in a smaller lattice size which is more suitable for trivalent ion conduction in the $Sc_2(WO_4)_3$-type structure. In $Sc_2(MoO_4)_3$, trivalent $Sc^{3+}$ ion conduction was also demonstrated by dc electrolysis to be similar to the case for $Sc_2(WO_4)_3$. Deposits of only Sc were recognized at the cathodic surface after electrolysis, while that observed for $Sc_2(WO_4)_3$ had cathodic deposits consisting of both Sc and W. The result indicates that the $Sc^{3+}$ cation migrated into the $Sc_2(MoO_4)_3$ and deposited at the cathodic surface where the Pt blocking electrode was in contact and consequently the deposited Sc metal was oxidized. However, the scandium oxide did not react with the mother bulk $Sc_2(MoO_4)_3$. This behavior is quite different from the case for $Sc_2(WO_4)_3$, since Sc was left in an oxide state.

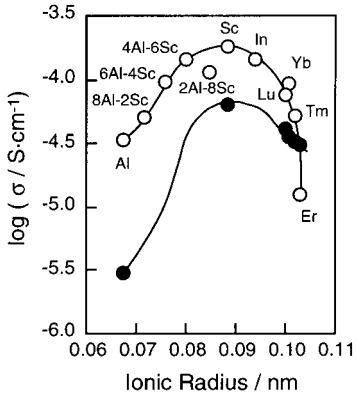


**Figure 42.** $M^{3+}$ ionic radius dependencies of the electrical conductivity at 600 °C for the tungstates (●) and the molybdates (○) with $Sc_2(WO_4)_3$-type structure. (Reprinted with permission from ref 131. Copyright 2000 American Chemical Society.)

From dc electrolysis, molybdates with $Sc_2(WO_4)_3$-type structure were clearly shown to be trivalent cation conductors, but molybdates were easily reduced compared with tungstates; e.g., $Sc_2(WO_4)_3$ is not reduced even at the partial oxygen pressure of $10^{-17}$ Pa, while $Sc_2(MoO_4)_3$ is reduced even at $10^{-13}$ Pa at 700 °C (as shown in Figure 43).

## E. NASICON-Type Structures

NASICON is one of the high $Na^+$ ion conducting solid electrolytes as well as $Na^+-\beta''$-alumina. The structure has a three-dimensional network where $PO_4$ tetrahedra and $ZrO_6$ octahedra are linked by

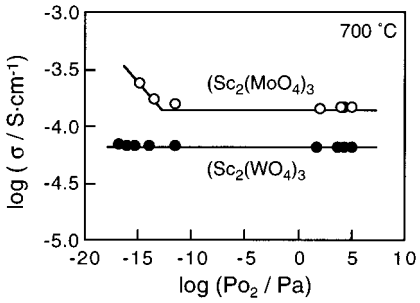


**Figure 43.** Oxygen partial pressure dependencies of the electrical conductivity for $Sc_2(WO_4)_3$ (●) and $Sc_2(MoO_4)_3$ (○). (Reprinted with permission from ref 131. Copyright 2000 American Chemical Society.)

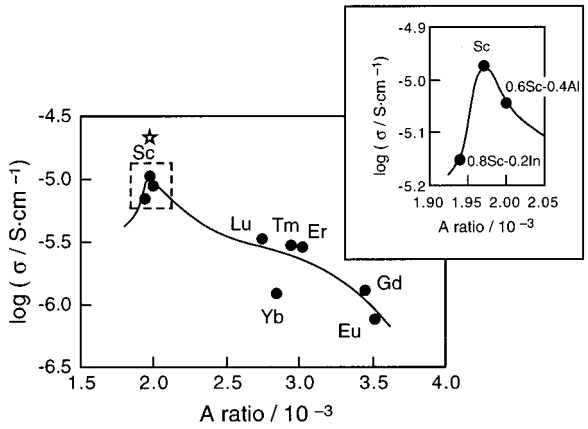


**Figure 44.** *A* ratio dependencies of the electrical conductivity for the $R_{1/3}Zr_2(PO_4)_3$ series which were prepared by a sol−gel method at 600 °C and $Sc_{1/3}Zr_2(PO_4)_3$ obtained by a ball milling method (☆). (Reprinted with permission from ref 139. Copyright 2001 Elsevier B.V.)

sharing an oxygen, which is well-known as one of the suitable structures for ion conduction. In 1994, Talbi et al.[147] reported that $Ln_{1/3}Zr_2(PO_4)_3$ (Ln = rare earths) with the NASICON-type structure could be prepared by a sol−gel method. However, the $Ln^{3+}$ cations contained in these materials are limited for some lanthanide atoms and ionic conducting characteristics were not investigated at all.

In 1999, $Sc_{1/3}Zr_2(PO_4)_3$ with NASICON-type structure was prepared and the $Sc^{3+}$ conducting behavior was investigated. For realizing the high trivalent cationic conduction, the *A* ratio (= conducting ion size/lattice size) was introduced in order to develop a solid electrolyte with an appropriate conducting pathway size in the lattice. The *A* ratio in $R_{1/3}Zr_2(PO_4)_3$ monotonically decreases with decreasing $Ln^{3+}$ radius, and only $Sc_{1/3}Zr_2(PO_4)_3$ shows a smaller *A* ratio compared to monovalent $Li^+$ conducting $LiTi_2(PO_4)_3$, which was reported to show the highest $Li^+$ conductivity among $Li^+$ conducting NASICON-type solid electrolytes. Since the electrostatic interaction between the mobile trivalent ion and surrounding oxide anions becomes stronger compared with the monovalent $Li^+$ ion and oxide anions, the optimum *A* ratio for the trivalent ion conduction in the NASICON-type structure should be smaller than that for the monovalent $Li^+$ ion conducting NASICON. Therefore, high conductivity is expected for $Sc_{1/3}Zr_2(PO_4)_3$. Figure 44 shows the *A* ratio dependencies of the electrical conductivity for $R_{1/3}Zr_2(PO_4)_3$, which were prepared by a sol−gel method, at 600 °C. As expected, $Sc_{1/3}Zr_2(PO_4)_3$ possessed the smallest *A* ratio and showed the highest conductivity among $R_{1/3}Zr_2(PO_4)_3$. A further detailed investigation of the relationship between the *A* ratio and the conductivity was carried out by preparing other solid solutions whose *A* ratios were similar to that of $Sc_{1/3}Zr_2(PO_4)_3$ (the result is shown as the insert in Figure 44). From the measurements, both conductivities of $0.6Sc_{1/3}Zr_2(PO_4)_3-0.4Al_{1/3}Zr_2(PO_4)_3$ and $0.8Sc_{1/3}Zr_2(PO_4)_3-0.2In_{1/3}Zr_2(PO_4)_3$ were lower than that of $Sc_{1/3}Zr_2(PO_4)_3$, and the highest trivalent conductivity is achieved for $Sc_{1/3}Zr_2(PO_4)_3$ (demonstration of trivalent $Sc^{3+}$ ion conduction in $Sc_{1/3}Zr_2(PO_4)_3$ is described below) in trivalent cation conducting NASICON-type solid electrolytes.

The $Sc_{1/3}Zr_2(PO_4)_3$ solid was demonstrated to be a $Sc^{3+}$ ion conductor by applying various experimental methods applied to the above-mentioned tungstate solid electrolytes. The ac conductivity maintained a constant value while the $O_2$ partial pressure was varied, indicating that no electronic conduction appears. The polarization behaviors in both $O_2$ and He atmospheres were similarly observed, and the transference number, $t_{ion}$, was estimated to be 0.95 from the $\sigma_{dc}/\sigma_{ac}$ ratio after 30 min. dc electrolysis was also performed in order to directly demonstrate which cation migrates in the solid. After dc electrolysis applying a dc voltage of 3V at 700 °C for 400 h, deposits were recognized at the cathodic surface. The deposits were identified by EPMA to be materials whose Sc/(Sc+Zr+P) ratio increased approximately 7.6 times as much as that in the bulk before electrolysis. These results explicitly indicate that $Sc^{3+}$ ions were found to migrate to the cathodic side by the electrolysis and deposited on the cathodic surface, and the mobile cationic species in $Sc_{1/3}Zr_2(PO_4)_3$ is identified to be $Sc^{3+}$ ions.

However, the conductivity ($1.07 \times 10^{-5}$ S·cm$^{-1}$ at 600 °C) of $Sc_{1/3}Zr_2(PO_4)_3$ prepared by a sol−gel method was low in comparison with that ($3.74 \times 10^{-5}$ S·cm$^{-1}$ at 600 °C) of $Sc^{3+}$ conducting $Sc_2(WO_4)_3$ tungstate since $Sc_{1/3}Zr_2(PO_4)_3$ obtained by a sol−gel method possessed a low crystallinity. In addition, the crystallization (ca. 800 °C) and the decomposition temperatures (ca. 950 °C) of $Sc_{1/3}Zr_2(PO_4)_3$ prepared by a sol−gel method are close, and improvement of the crystallinity seems to be difficult by a conventional sol−gel method. Furthermore, it is very difficult to prepare the $Sc_{1/3}Zr_2(PO_4)_3$ solid electrolyte by a conventional solid-state reaction because the energy for the solid-state reaction cannot be supplied enough at the temperature below the decomposition temperature of 950 °C. To enhance the crystallinity of $Sc_{1/3}Zr_2(PO_4)_3$, the ball milling method was applied for the synthesis. The ball milling method can mix the starting powder with a strong force and make the powder form an amorphous phase by applying a high mechanical energy and is expected to be effective to obtain a high crystallization of the $Sc_{1/3}Zr_2(PO_4)_3$ series. The crystallinity of $Sc_{1/3}Zr_2(PO_4)_3$ was greatly enhanced, and the $Sc^{3+}$ ion conductivity increased up to $2.91 \times 10^{-5}$ S·cm$^{-1}$ at 600 °C (☆), as shown in Figure 44. The conductivity of $Sc_{1/3}Zr_2(PO_4)_3$ prepared

by a ball mill method is found to be comparable to the series of $Sc_2(WO_4)_3$-type structures, especially at 600 °C. The activation energy for ion conduction in $Sc_{1/3}Zr_2(PO_4)_3$ prepared by a ball mill method, which is derived from the relationship between $\log(\sigma T)$ and $1/T$, is 72.7 kJ·mol$^{-1}$. This value is a little higher than those of $Sc_2(WO_4)_3$ (56.4 kJ·mol$^{-1}$) and $Al_2(WO_4)_3$ (65.8 kJ·mol$^{-1}$), indicating that a similar suitable ion pathway was achieved in both NASICON and $Sc_2(WO_4)_3$-type structures.

$Sc_{1/3}Zr_2(PO_4)_3$ has another advantage compared with $Sc_2(WO_4)_3$. Table 3 shows the trivalent ion conductivity at 600 °C, Vickers hardness, and relative density for $Sc_{1/3}Zr_2(PO_4)_3$ (both sol−gel and ball mill methods) and $Sc_2(WO_4)_3$, which shows the highest trivalent ion conductivity in the $Sc_2(WO_4)_3$-type series. The relative densities of both $Sc_{1/3}Zr_2(PO_4)_3$ solid electrolytes are considerably higher than $Sc_2(WO_4)_3$. In addition, the Vickers hardness of the $Sc_{1/3}Zr_2(PO_4)_3$ solid electrolyte is more than 7 times as high as that of $Sc_2(WO_4)_3$. The results described above clearly indicate the fact that the $Sc_{1/3}Zr_2(PO_4)_3$ solid electrolyte based on a phosphate framework was successfully obtained with having a high relative density and a considerable high mechanical hardness which may serve as a useful property in its application for various types of devices.

**Table 3. Trivalent $Sc^{3+}$ Ion Conductivity, Vickers Hardness, and Relative Density for $Sc_2(WO_4)_3$ and $Sc_{1/3}Zr_2(PO_4)_3$**

| $Sc^{3+}$ ion conductors | conductivity ($\sigma$/S cm$^{-1}$) | Vickers hardness (Hv) | relative density (%) |
|---|---|---|---|
| $Sc_2(WO_4)_3$ | $3.74 \times 10^{-5}$ | 40 | 89 |
| $Sc_{1/3}Zr_2(PO_4)_3$ (sol−gel) | $1.07 \times 10^{-5}$ | 293 | 99.9 |
| $Sc_{1/3}Zr_2(PO_4)_3$ (ball mill) | $2.91 \times 10^{-5}$ | 305 | 99.9 |

## V. Concluding Remarks

Rare-earth (including lanthanoid) elements have been widely applied in the solid state ionics field. Generally by holding the trivalent state stable, the doping of rare earths (including lanthanoids) to improve the ion conducting characteristics has been the main direction of investigation. In this case, the rare-earth contribution is only as additives. One exception is lanthanum fluoride ($LaF_3$), which is a main component of the solid electrolyte, and as the doping element, divalent europium cation is also added as additives to form a solid solution. Other representative exceptions are proton conducting cerates solid electrolyte based on perovskite-type and oxide anion conducting fluorite-type cerium dioxide. The perovskite-type structure is a very attractive framework which contributes not only in the field of Solid State Ionics but also as metallic, semiconducting materials and dielectrics, and the structure "perovskite" is an interdisciplinary framework in solid state chemistry. However, as described above, both oxide series contain $Ce^{4+}$ ions in them, and due to the properties of their easy reduction nature, the application fields are very limited.

In 1995, trivalent rare-earth macroscopic ion migration in solids was demonstrated. Since 1995, the rare-earth (including lanthanoids) cations have become one of main players in the solid electrolyte field. Among the Sc, Y, and lanthanoids series composed of 17 elements, the most stable valency is the trivalent state. Therefore, the rare-earth ion migration in solids is mainly cations with a trivalent state. However, some rare earths have divalent or tetravalent states, and there exists some expectation of developing another solid electrolyte where divalent or tetravalent rare-earth ions can macroscopically migrate. If this comes true soon, the field will expand immensely and unexpected applications may be realized in the future. For success, selection of the structure and the combination of the constituent elements will be an important factor.

## VI. Acknowledgment

The authors thank Professor Dr. Richard A. Secco, Department of Earth Science, University of Western Ontario, for prereviewing the article.

## VII. References

(1) Warburg, E.; Tegetmeier, F. **1888**, *32*, 455.
(2) Wagner, C. *Naturwissenschaften* **1943**, *31*, 265.
(3) Tubandt, C. Z. *Anorg. Allg. Chem*. **1921**, *115*, 105.
(4) Bradley, J. N.; Greene, P. D. *Trans. Faraday* **1965**, *62*, 2069.
(5) Frant, M. S.; Ross, Jr., J. W. *Science* **1966**, *154*, 1553.
(6) Weber, N.; Kummer, J. T. *Proc. Ann. Power Sources Conf*. **1967**, *21*, 37.
(7) Goodenough, J. B.; Hong, H. Y−P.; Kafalas, J. A. *Mater. Res. Bull*. **1976**, *11*, 203.
(8) Iwahara, H.; Uchida, H.; Maeda, N. *J. Power Sources* **1982**, *7*, 293.
(9) Adachi, G.; Imanaka, N. *Inorganic Chemical Highlights*; Meyer, G., et al., Eds.; Wiley-VCH, in press.
(10) Köhler, J.; Imanaka, N.; Adachi, G. *Chem. Mater*. **1998**, *10*, 3790.
(11) Latie, L.; Villeneuve, G.; Conte, D.; Flem. G. L. *J. Solid State Chem*. **1984**, *51*, 293.
(12) Inaguma, Y.; Matsui, Y.; Yu, J.; Shan, Y.; Nakamura, T.; Itoh, M. *J. Phys. Chem. Solids* **1997**, *58*, 843.
(13) Itoh, M.; Inaguma, Y.; Jung, W.-H.; Nakamura, T. *Solid State Ionics* **1994**, *70/71*, 203.
(14) Katsumata, T.; Inaguma, Y.; Itoh, M.; Kawamura, K. *J. Ceram. Soc. Jpn*. **1999**, *107*, 615.
(15) Stauffer, D.; Aharony, A. *Introduction to Percolation theory*, 2nd ed.; Taylor and Francis: London, 1992.
(16) Inaguma, Y.; Liquan, C.; Itoh, M.; Nakamura, T. *Solid State Commun*. **1993**, *86*, 689.
(17) Kawai, H.; Kuwano, J. *J. Electrochem. Soc*. **1994**, *141*, L78.
(18) Inaguma, Y.; Chan, L.; Itoh, M.; Nakamura, T. *Solid State Ionics* **1994**, *70/71*, 196.
(19) Inaguma, Y.; Itoh, M. *Solid State Ionics* **1996**, *86−88*, 257.
(20) Dyer, A. J.; White, E. A. D. *Trans. Br. Ceram. Soc*. **1964**, *63*, 301.
(21) Iyer, P. N.; Smith, A. J. *Acta Crystallogr*. **1967**, *23*, 740.
(22) Sato, M.; Kono, Y.; Uematsu, K. *Chem. Lett*. **1994**, 1425.
(23) Sato, M.; Kono, Y.; Ueda, H.; Uematsu, K.; Toda, K. *Solid State Ionics* **1996**, *83*, 249.
(24) Matsumoto, H.; Yonezawa, K.; Iwahara, H. *Solid State Ionics* **1998**, *113−115*, 79.
(25) Esaka, T.; Kobayashi, Y.; Obata, H.; Iwahara, H. *Solid State Ionics* **1989**, *34*, 287.
(26) Shannon, R. D. *Acta Crystallogr. A* **1976**, *32*, 751.
(27) Adachi, G.; Imanaka, N. *Handbook on the Physics and Chemistry of Rare Earths*; 1995: Vol. 21, p 179.
(28) Uchida, H.; Maeda, N.; Iwahara, H. *Solid State Ionics* **1983**, *11*, 117.
(29) Shimojo, F.; Hoshino, K.; Okazaki, H. *Solid State Ionics* **1998**, *113−115*, 319.
(30) Shimojo, F.; Hoshino, K.; Okazaki, H. *J. Phys. Soc. Jpn*. **1998**, *67*, 2008.
(31) Hempelmann, R.; Karmonik, Ch. *Phase Transitions* **1996**, *58*, 175.
(32) Liang, K. C.; Du, Y.; Nowick, A. S. *Solid State Ionics* **1994**, *69*, 117.
(33) Schwartz, M.; Link, B. F.; Sammells, A. F. *J. Electrochem. Soc*. **1993**, *140*, L62.

(34) Shimura, T.; Komori, M.; Iwahara, H. *Solid State Ionics* **1996**, *86−88*, 685.
(35) Ghosal, B.; Mangle, E. A.; Topp, M. R.; Dunn, B.; Farrington, G. C. *Solid State Ionics* **1983**, *9/10*, 273.
(36) Wen, Z.-Y.; Lin, Z.-X.; Tian, S.-B. *Solid State Ionics* **1990**, *40/41*, 91.
(37) Dunn, B.; Farrington, G. C. *Solid State Ionics* **1983**, *9/10*, 223.
(38) Imanaka, N.; Okamoto, K.; Adachi, G. *Chem. Lett.* **2001**, 130.
(39) Inaba, H.; Tagawa, H. *Solid State Ionics* **1996**, *83*, 1.
(40) Kudo, T.; Obayashi, H. *J. Electrochem. Soc.* **1975**, *122*, 142.
(41) Huang, W.; Shuk, P.; Greenblatt, M. *Chem. Mater.* **1997**, *9*, 2240.
(42) Huang, W.; Shuk, P.; Greenblatt, M. *J. Electrochem. Soc.* **2000**, *147*, 439.
(43) Huang, W.; Shuk, P.; Greenblatt, M. *Solid State Ionics* **1998**, *113−115*, 305.
(44) Alcock, C. B.; Fergus, J. W.; Wang, L. *Solid State Ionics* **1992**, *51*, 291.
(45) Takahashi, T.; Iwahara, H. *Energy Convers.* **1971**, *11*, 105.
(46) Ishihara, T.; Matsuda, H.; Takita, Y. *J. Electrochem. Soc.* **1994**, *141*, 3444.
(47) Cook, R. L.; Sammells, A. F. *Solid State Ionics* **1991**, *45*, 311.
(48) Ishihara, T.; Matsuda, H.; Takita, Y. *J. Am. Chem. Soc.* **1994**, *116*, 3801.
(49) Ishihara, T.; Matsuda, H.; Takita, Y. *Solid State Ionics* **1995**, *79*, 147.
(50) Ishihara, T.; Hiei, Y.; Takita, Y. *Solid State Ionics* **1995**, *79*, 371.
(51) Cook, R. L.; MacDuff, R. C.; Sammells, A. F. *J. Electrochem. Soc.* **1990**, *137*, 3309.
(52) Lacorre, P.; Goutenoire, F.; Bohnke, O.; Retoux, R.; Laligant, Y. *Nature* **2000**, *404*, 856.
(53) Goutenoire, F.; Isnard, O.; Retoux, R. Lacorre, P. *Chem. Mater.* **2000**, *12*, 2575.
(54) Takashima, M. *Advances in Inorganic Fluoride: Synthesis, Characterization and Applications*; Nakajima, T., Zemva, B., Tressaud, A., Eds.; Elsevier Science S.A.: Lausanne, 2000; p 175.
(55) Takashima, M.; Yonezawa, S.; Tanioka, T.; Nakajima, Y.; Leblanc, M. *Solid State Sci.* **2000**, *2*, 71.
(56) Takashima, M. *J. Fluorine Chem.* **2000**, *105*, 249.
(57) Takashima, M.; Kano, G. *Solid State Ionics* **1987**, *23*, 99.
(58) Takashima, M.; Kanoh, G.; Kawase, *M. Denki Kagaku* **1985**, *53*, 2.
(59) Milne, S. J.; Brook, R. J.; Zhen, Y. S. *Br. Ceram. Proc.* **1989**, *41*, 243.
(60) Sammells, A. F.; Cook R. L.; White, J. H.; Osborne, J. J.; MacDuff, R. C. *Solid State Ionics* **1992**, *52*, 111.
(61) Goodenough, J. B.; Ruiz-Diaz, J. E.; Zhen, Y. S. *Solid State Ionics* **1990**, *44*, 21.
(62) Uematsu, K.; Shinozaki, K.; Sakurai, O.; Mizutani, N.; Kato, M. *J. Am. Ceram. Soc.* **1979**, *62*, 219.
(63) Shinozaki, K.; Miyauchi, M.; Kuroda, K.; Sakurai, O.; Mizutani, N.; Kato, M. *J. Am. Ceram. Soc.* **1979**, *62*, 538.
(64) Dijk, T.; Vries, K. J.; Burggraaf, A. J. *Phys. Status Solidi A* **1980**, *58*, 115
(65) Pawlowski, A.; Hilczer, B. *Key Eng. Mater.* **1998**, *155−156*, 199.
(66) Tuller, H.; Moon, P. K. *Mater. Sci. Eng.* **1988**, *B1*, 171.
(67) Kumar, R. V.; Iwahara, H. *Handbook on the Physics and Chenistry of Rare Earths;* 2000; Vol. 28, p 131.
(68) Subramanian, M. A.; Subramanian, R.; Clearfield, A. *Solid State Ionics* **1986**, *18/19*, 562.
(69) Aono, H.; Sugimoto, E.; Sadaoka, Y.; Imanaka, N.; Adachi, G. *J. Electrochem. Soc.* **1989**, *136*, 590.
(70) Aono, H.; Sugimoto, E.; Sadaoka, Y.; Imanaka, N.; Adachi, G. *J. Electrochem. Soc.* **1990**, *137*, 1023.
(71) Aono, H.; Sugimoto, E.; Sadaoka, Y.; Imanaka, N.; Adachi, G. *Solid State Ionics* **1990**, *40/41*, 38.
(72) Thangadurai, V.; Shukla, A. K.; Gopalakrishnan, J.; Joubert, O.; Brohan, L.; Tournoux, M. *Mater. Sci. Forum* **2000**, *321−324*, 965.
(73) Shannon, R. D.; Taylor, B. E.; Gier, T. E.; Chen, H.-Y.; Berzins, T. *Inorg. Chem.* **1978**, *17*, 958.
(74) Imanaka, N.; Adachi, G.; Shiokawa, J. *Bull. Chem. Soc. Jpn.* **1984**, *57*, 687.
(75) Imanaka, N.; Yamaguchi, Y.; Adachi, G.; Shiokawa, J. *Solid State Ionics* **1986**, *20*, 153.
(76) Imanaka, N.; Kuwabara, S.; Adachi, G.; Shiokawa, J. *Solid State Ionics* **1987**, *23*, 15.
(77) Imanaka, N.; Yamaguchi, Y.; Adachi, G.; Shiokawa, J. *Bull. Chem. Soc. Jpn.* **1985**, *58*, 5.
(78) Imanaka, N.; Yamaguchi,; Y. Adachi, G.; Shiokawa, J. *J. Electrochem. Soc.* **1986**, *133*, 1026.
(79) Sata, N.; Hiramoto, K.; Ishigame, M. *Phys. Rev. B* **1996**, *54*, 15795.
(80) Huang, H. H.; Ishigame, M.; Shin, S. *Solid State Ionics* **1991**, *47*, 251.
(81) Shin, S.; Huang, H. H.; Ishigame, M. *Solid State Ionics* **1990**, *40/41*, 910.
(82) Cook, R. L.; Osborne, J. J.; White, J. H.; MacDuff, R. C.; Sammells, A. F. *J. Electrochem. Soc.* **1992**, *139*, L19.
(83) Nernst, W. Z. *Electrochem.* **1899**, *6*, 41.
(84) Etsell, T. H.; Flengas, S. N. *Chem. Rev.* **1970**, *70*, 339.
(85) Kharton, V. V.; Naumovich, E. N.; Vecher, A. A. *J. Solid State Electrochem.* **1999**, *3*, 61.
(86) Badwal, S. P. S.; Ciacchi, F. T.; Rajendran, S.; Drennan, J. *Solid State Ionics* **1998**, *109*, 167.
(87) Sammes, N. M.; Tompsett, G. A.; Näfe, H.; Aldinger, F. *J. Eur. Ceram. Soc.* **1999**, *19*, 1801.
(88) Azad, A. M.; Larose, S.; Akbar, S. A. *J. Mater. Sci.* **1994**, *29*, 4135.
(89) Weyl, A.; Janke, D. *J. Am. Ceram. Soc.* **1996**, *79*, 2145.
(90) Yamashita, K.; Owada, H.; Umegaki, T.; Kanazawa, T.; Futagami, T. *Solid State Ionics* **1988**, *28−30*, 660.
(91) Nakayama, S.; Aono, H.; Sadaoka, Y. *Chem. Lett.* **1995**, 431.
(92) Nakayama, S.; Kageyama, T.; Aono, H.; Sadaoka, Y. *J. Mater. Chem.* **1995**, *5*, 1801.
(93) Sansom, J. E. H.; Richings, D.; Slater, P. R. *Solid State Ionics* **2001**, *139*, 205.
(94) Abram, E. J.; Sinclair, D. C.; West, A. R. *J. Mater. Chem.* **2001**, *11*, 1978.
(95) Sattar, S.; Ghosal, B.; Underwood, M. L.; Mertwoy, H.; Saltzberg, M. A.; Frydrych, W. S.; Rohrer, G. S.; Farrington, G. C. *J. Solid State Chem.* **1986**, *65*, 231.
(96) Farrington, G. C.; Dunn, B.; Thomas, J. O. *Appl. Phys. A* **1983**, *32*, 159.
(97) Köhler, J.; Urland, W. *Z. Anorg. Allg. Chem.* **1997**, *623*, 231.
(98) Köhler, J.; Urland, W. *Z. Anorg. Allg. Chem.* **1996**, *622*, 191.
(99) Köhler, J.; Urland, W. *J. Solid State Chem.* **1996**, *127*, 161.
(100) Köhler, J.; Urland, W. *Solid State Ionics* **1996**, *86−88*, 93.
(101) Tietz, F.; Urland, W. *Solid State Ionics* **1995**, *78*, 35.
(102) Köhler, J.; Urland, W. *Angew. Chem., Int. Ed.* **1997**, *36*, 85.
(103) Köhler, J.; Imanaka. N.; Urland, W.; Adachi. G. *Angew. Chem., Int. Ed.* **2000**, *39*, 904.
(104) Yang, D. L.; Dunn, B.; Morgan, P. E. D. *J. Mater. Sci. Lett.* **1991**, *10*, 485.
(105) Tietz, F.; Urland, W. *Solid State Ionics* **1991**, *46*, 331.
(106) Tietz, F.; Urland, W. *J. Alloys Compd.* **1993**, *192*, 78.
(107) Tietz, F.; Urland, W. *J. Solid State Chem.* **1992**, *100*, 255.
(108) Wang, X. E.; Lejus, A. M.; Vivien, D.; Collongues, R. *Mater. Res. Bull.* **1988**, *23*, 43.
(109) Sun, W. Y.; Yen, T. S.; Tien, T. Y. *J. Solid State Chem.* **1991**, *95*, 424.
(110) Kahn, A.; Lejus, A. M.; Madsac, M.; Théry, J.; Vivien, D.; Bernier, J. C. *J. Appl. Phys.* **1981**, *52*, 6864.
(111) Warner, T. E.; Fray, D. J.; Davies, A. *Solid State Ionics* **1996**, *92*, 99.
(112) Warner, T. E.; Fray, D. J.; Davies, A. *J. Mater. Sci.* **1997**, *32*, 279.
(113) George, A. M.; Virkar, A. N. *J. Phys. Chem. Solids* **1988**, *49*, 743.
(114) Imanaka, N.; Kobayashi, Y.; Adachi, G. *Chem. Lett.* **1995**, 433.
(115) Kobayashi, Y.; Egawa, T.; Tamura, S.; Imanaka, N.; Adachi, G. *Chem. Mater.* **1997**, *9*, 1649.
(116) Imanaka, N.; Kobayashi, Y.; Tamura, S.; Adachi, G. *Electrochem. Solid-State Lett.* **1998**, *1*, 271.
(117) Kobayashi, Y.; Egawa, T.; Okazaki, Y.; Tamura, S.; Imanaka, N.; Adachi, G. *Solid State Ionics* **1998**, *111*, 59.
(118) Tamura, S.; Egawa, T.; Okazaki, Y.; Kobayashi, Y.; Imanaka, N.; Adachi, G. *Chem. Mater.* **1998**, *10*, 1958.
(119) Imanaka, N.; Kobayashi, Y.; Fujiwara, K.; Asano, T.; Okazaki, Y.; Adachi, G. *Chem. Mater.* **1998**, *10*, 2006.
(120) Imanaka, N.; Hiraiwa, M.; Tamura, S.; Adachi, G.; Dabkowska, H.; Dabkowski, A.; Greedan, J. E. *Chem. Mater.* **1998**, *10*, 2542.
(121) Imanaka, N.; Adachi, G. *Molten Salts* **1998**, *41*, 177.
(122) Kobayashi, Y.; Tamura, S.; Imanaka, N.; Adachi, G. *Solid State Ionics* **1998**, *113−115*, 545.
(123) Köhler, J.; Kobayashi, Y.; Imanaka, N.; Adachi, G. *Solid State Ionics* **1998**, *113−115*, 553.
(124) Kobayashi, Y.; Egawa, T.; Tamura, S.; Imanaka, N.; Adachi, G. *Solid State Ionics* **1999**, *118*, 325.
(125) Köhler, J.; Imanaka, N.; Adachi, G. *Solid State Ionics* **1999**, *122*, 173.
(126) Köhler, J.; Imanaka, N.; Adachi, G. *Z. Anorg. Allg. Chem.* **1999**, *625*, 1890.
(127) Imanaka, N.; Hiraiwa, M.; Tamura, S.; Adachi, G. *Electrochem. Solid-State Lett.* **1999**, *2*, 570.
(128) Imanaka, N.; Tamura, S.; Adachi, G.; Kowada, Y. *Solid State Ionics* **2000**, *130*, 179.
(129) Okazaki, Y.; Ueda, T.; Tamura, S.; Imanaka, N.; Adachi, G. *Solid State Ionics* **2000**, *136/137*, 437.
(130) Köhler, J.; Imanaka, N.; Adachi, G. *Solid State Ionics* **2000** *136/137*, 431.
(131) Imanaka, N.; Ueda, T.; Okazaki, Y.; Tamura, S.; Adachi, G. *Chem. Mater.* **2000**, *12*, 1910.
(132) Adachi, G.; Imanaka, N.; Tamura, S. *J. Alloys Compd.* **2001**, *323/324*, 534.
(133) Secco, R. A.; Liu, H.; Imanaka, N.; Adachi, G.; Rutter, M. D. *J. Phys. Chem. Solids*, in press.

(134) Imanaka, N.; Köhler, J.; Tamura, S.; Adachi, G. *Eur. J. Inorg. Chem*., in press.
(135) Tamura, S.; Imanaka, N.; Adachi, G. *Adv. Mater*. **1999**, *11*, 1521.
(136) Tamura, S.; Imanaka, N.; Adachi, G. *Solid State Ionics* **2000**, *136/137*, 423.
(137) Tamura, S.; Imanaka, N.; Adachi, G. *J. Alloys Compd*. **2001**, *323/324*, 540.
(138) Tamura, S.; Imanaka, N.; Adachi, G. *Chem. Lett*. **2001**, 672.
(139) Imanaka, N.; Adachi, G. *J. Alloys Compd*., in press.
(140) Foster, L. M.; Arbach, G. V. *J. Electrochem. Soc*. **1977**, *124*, 164.
(141) Foster, L. M.; Stumpf, H. C. *J. Am. Chem. Soc*. **1973**, *73*, 1590.
(142) Sakai, N.; Toda, K.; Sato, M. *Electrochemistry* **2000**, *68*, 504.
(143) Studer, F.; Montfort, Y.; Raveau, B. *J. Solid State Chem*. **1973**, *7*, 269.
(144) Desgardin, G.; Raveau, B. *J. Inorg. Nucl. Chem*. **1973**, *35*, 2295.
(145) Ebisu, S.; Morita, H.; Nagata, S. *J. Phys. Chem. Solids* **2000**, *61*, 45.
(146) Nassau, K.; Shiever, J. W.; Keve, E. T. *J. Solid State Chem*. **1971**, *3*, 411.
(147) Talbi, M. A.; Brochu, R.; Parent, C.; Rabardel, L.; Flem, G. L. *J. Solid State Chem*. **1994**, *110*, 350.

CR0103064